EDGEWOOD CHEMICAL BIOLOGICAL CENTER
U.S. ARMY RESEARCH, DEVELOPMENT AND ENGINEERING COMMAND
Aberdeen Proving Ground, MD 21010-5424

ECBC-TR-1202

MODELING FOR STANDOFF SURFACE DETECTION

Raphael P. Moon
Steven D. Christesen

RESEARCH AND TECHNOLOGY DIRECTORATE

Kevin Hung

HUNG TECHNOLOGY SOLUTIONS, LLC
Baltimore, MD 21234-2601

Paul Corriveau

ITT CORPORATION
Edgewood, MD 21040-1125

Norman Green

SCIENCE AND TECHNOLOGY CORPORATION
Edgewood, MD 21040-2734

November 2013

Approved for public release; distribution is unlimited.

U.S. ARMY RDECOM

Disclaimer

The findings in this report are not to be construed as an official Department of the Army position unless so designated by other authorizing documents.

REPORT DOCUMENTATION PAGE

Form Approved
OMB No. 0704-0188

Public reporting burden for this collection of information is estimated to average 1 h per response, including the time for reviewing instructions, searching existing data sources, gathering and maintaining the data needed, and completing and reviewing this collection of information. Send comments regarding this burden estimate or any other aspect of this collection of information, including suggestions for reducing this burden to Department of Defense, Washington Headquarters Services, Directorate for Information Operations and Reports (0704-0188), 1215 Jefferson Davis Highway, Suite 1204, Arlington, VA 22202-4302. Respondents should be aware that notwithstanding any other provision of law, no person shall be subject to any penalty for failing to comply with a collection of information if it does not display a currently valid OMB control number. **PLEASE DO NOT RETURN YOUR FORM TO THE ABOVE ADDRESS.**

1. REPORT DATE *(DD-MM-YYYY)*	2. REPORT TYPE	3. DATES COVERED *(From - To)*
XX-11-2013	Final	Oct 2008 – Sep 2012

4. TITLE AND SUBTITLE
Modeling for Standoff Surface Detection

5a. CONTRACT NUMBER

5b. GRANT NUMBER

5c. PROGRAM ELEMENT NUMBER

6. AUTHOR(S)
Moon, Raphael P.; Christesen, Steven D. (ECBC); Hung, Kevin (HTS); Corriveau, Paul (ITT); and Green, Norman (STC)

5d. PROJECT NUMBER
BA06DET018

5e. TASK NUMBER

5f. WORK UNIT NUMBER

7. PERFORMING ORGANIZATION NAME(S) AND ADDRESS(ES)
Director, ECBC, ATTN: RDCB-DRD-L, APG, MD 21010-5424
Hung Technology Solutions, LLC, 2611 Luiss Deane Drive, Baltimore, MD 21234-2601
ITT Corporation, 1109 Edgewood Road, Edgewood, MD 21040-1125
Science and Technology Corporation, 500 Edgewood Road, Suite 205, Edgewood, MD 21040-2734

8. PERFORMING ORGANIZATION REPORT NUMBER
ECBC-TR-1202

9. SPONSORING / MONITORING AGENCY NAME(S) AND ADDRESS(ES)
Defense Threat Reduction Agency, 8725 John J. Kingman Road, MSC 6201, Fort Belvoir, VA 22060-6201

10. SPONSOR/MONITOR'S ACRONYM(S)
DTRA

11. SPONSOR/MONITOR'S REPORT NUMBER(S)

12. DISTRIBUTION / AVAILABILITY STATEMENT
Approved for public release; distribution is unlimited.

13. SUPPLEMENTARY NOTES

14. ABSTRACT:

This report describes the development of a contamination droplet-distribution model generated from the output of the chemical and biological agent Vapor, Liquid, and Solid Tracking (VLSTRACK) computer model. VLSTRACK provides the approximate downwind hazard predictions, droplet distributions, and gross contamination levels for chemical agents and munitions of military interest. During this study, we also modeled generic standoff-detection systems using a point-scanning and imaging mode. We validated the models using laboratory measurements and a design of experiments approach.

15. SUBJECT TERMS
Standoff Detection
VLSTRACK
Modeling
Surface Detection

16. SECURITY CLASSIFICATION OF:			17. LIMITATION OF ABSTRACT	18. NUMBER OF PAGES	19a. NAME OF RESPONSIBLE PERSON
a. REPORT	b. ABSTRACT	c. THIS PAGE			Renu B. Rastogi
U	U	U	UU	70	19b. TELEPHONE NUMBER *(include area code)* (410) 436-7545

Blank

PREFACE

The work described in this report was authorized under project no. BA06DET018. The work was started in October 2008 and completed in September 2012.

The use of either trade or manufacturers' names in this report does not constitute an official endorsement of any commercial products. This report may not be cited for purposes of advertisement.

This report has been approved for public release.

Acknowledgments

The authors wish to acknowledge the Defense Threat Reduction Agency Joint Science and Technology Office for its funding of this project. We also want to express our appreciation for Dr. Ngai Wong's guidance and critical reviews of the project's goals and progress.

Blank

CONTENTS

FIGURES

TABLES

MODELING FOR STANDOFF SURFACE DETECTION

1. INTRODUCTION

In support of the technology-oriented components of the surface detection program, the U.S. Army Edgewood Chemical and Biological Command (ECBC) developed a model of the contaminated droplet distribution on surfaces using realistic values for the chemical fill and delivery system. For this effort, we relied on existing models that account for the fate and transport of agent aerosols in the atmosphere and on experimental data that describe the droplet distribution. The chemical and biological agent Vapor, Liquid, and Solid Tracking (VLSTRACK) computer model (U.S. Naval Surface Warfare Center, Dahlgren, VA) provided us with approximate downwind hazard predictions, droplet distributions, and gross contamination levels for chemical agents and munitions of military interest.

During this study, we also modeled generic standoff-detection systems using a point-scanning and imaging mode. We validated the models using laboratory measurements and a design of experiments (DoE) approach. The goal was a front-to-back modular model that allowed for virtual testing of detection systems and techniques (Figure 1).

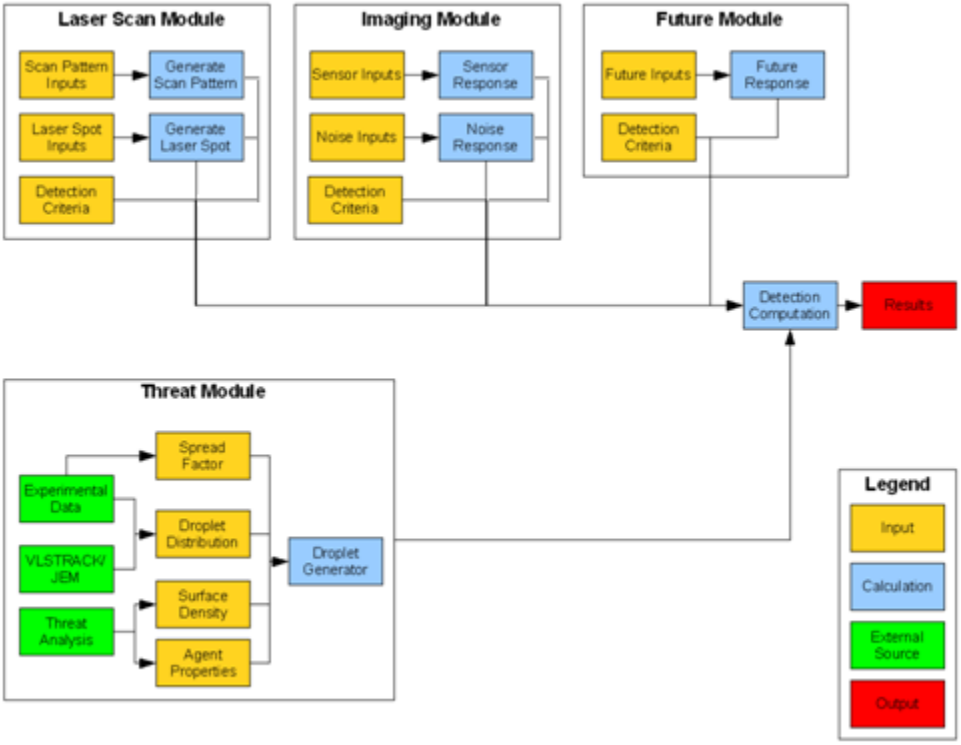

Figure 1. Model architecture.

2. OBJECTIVE

The overall objective of this program was to create a predictive model for standoff detection of chemicals on surfaces. Our efforts focused on developing validated modeling tools that will be used to specify surface contamination and evaluate potential detection and scanning technologies.

3. THREAT CONTAMINATION MODELING

3.1 VLSTRACK Description

VLSTRACK is an atmospheric hazard assessment model for chemical and biological warfare attacks. The computer model outputs concentration, dosage, and deposition values at selected spatial points downwind of a contaminant release depending on the agents disseminated. For atmospheric releases of chemical agents, VLSTRACK is used to predict droplet concentration, dosage, and deposition and vapor concentration and dosage. For biological agents, VLSTRACK is used to predict downwind particle concentration, dosage, and deposition.

VLSTRACK simulates the downwind transport and dispersion of atmospheric contaminants using the Gaussian Puff technique. After dissemination, airborne contaminants are represented as a collection of vapor, liquid, and solid puffs. Each puff has a Gaussian distribution, and each is modeled independently as it is transported downwind. Final values of concentration, dosage, and deposition are determined by adding the contributions from all of the puffs. In addition, VLSTRACK is used to model evaporation effects for liquid agents including blast vaporization, droplet evaporation, secondary evaporation from liquid deposition, and liquid desorption.

Bauer and Gibbs[1] provide further details concerning the modeling techniques and computer operation of VLSTRACK, examples of this computer model use, and instructions for interpreting the VLSTRACK model output.

3.2 Model Input Parameters

The VLSTRACK computer model requires several input parameter values to properly model downwind transport and dispersion. Meteorological parameters such as wind speed, wind direction, temperature, humidity, and the Pasquill stability class are required. In addition, physical and chemical properties of the agent including density, volatility, heat of vaporization, viscosity, surface tension, and vapor diffusivity must be input to the model.

Some input parameters are determined by the specific munition that is used to disseminate the agent. These include fill weight, number of submunitions, initial Gaussian Puff sigmas, and the droplet size distribution. For the latter, VLSTRACK incorporates a log-normal distribution and requires the mass median diameter (MMD) and geometric standard deviation.

When using VLSTRACK, the user is prompted to input the parameters listed in the previous paragraphs. However, if the user does not have access to actual measurements, the VLSTRACK computer model can provide default values that provide a good approximation of the required parameters. However, these default values are not considered to be validated; they are a consensus of various previous measurements on similar agents and munitions.

3.3 VLSTRACK Validation

Validation studies have been performed on the VLSTRACK computer model to determine its ability to accurately predict concentration, dosage, and deposition values downwind from an atmospheric release of contaminant (usually an agent simulant). These studies generally involved field experiments that were designed to measure quantities predicted by VLSTRACK, together with other required measurements such as meteorological parameters. The experimentally measured quantities were then compared with those predicted using VLSTRACK.

In total, the VLSTRACK validation results were based on a statistical comparison with 7745 data points from 60 field-trial experiments. Results of these validation studies are presented by Bauer and Gibbs.[2] As indicated in this report, VLSTRACK was used to predict concentration, dosage, and deposition values that were in good agreement with the experimentally measured values. On average, the VLSTRACK predictions were 27% higher than the field-trial observations. In addition, 37% of the VLSTRACK predictions were within a factor of 2, and 52% of the cases were within a factor of 3 of the field observations.

4. SURFACE DETECTION MODELING AND SIMULATION

4.1 Background

For this project, we coded a model that simulates a laser scan of a contaminated surface. The flow chart in Figure 2 shows the implementation of the laser-scan module, which was intended to facilitate the design and optimization of a laser-based detection system for determining the presence of surface contamination. In addition to being laser-based, the model is detection-technology-independent and utilizes object-oriented design to ensure interoperability with independently developed detection models. The model first generates the contaminated surface, scans that surface, and then outputs the scan results. For a given surface type, threat material, and source term, the model provides a pattern of contamination on the surface that is consistent with the atmospheric conditions and takes into account the physical parameters associated with liquid deposition. The model then invokes one of several scan patterns to interrogate the surface. The scan pattern module includes the appropriate representation of a laser-based scanner and searches for instances where the simulated laser spots are coincident with the deposited contamination. The model is modular, and a wide variety of parameters can be modified to simulate multiple scenarios. Numerous subfunctions are coded as separate files that can be replaced with substitutes to vary functionality.

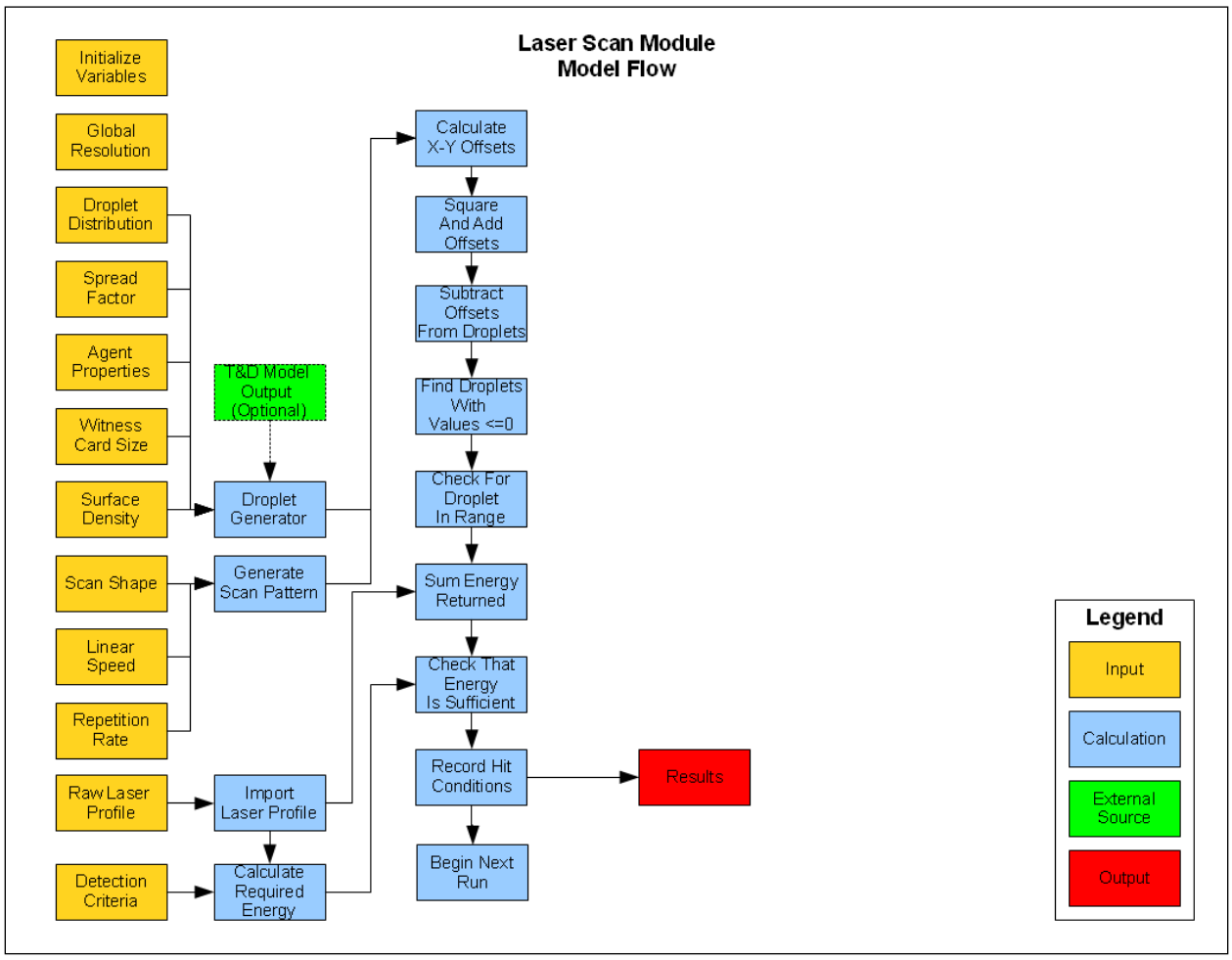

Figure 2. Model flowchart.

The core of the model is the hit-detection portion, which scans the laser across the contamination and returns results. The entirely digital model stores all points as pixels with integer *x*–*y* coordinates, which allows for easier comparison of matrices by checking for integer equality. This digitization is conducted by setting a global resolution and rounding all numbers to the closest pixel.

A DoE approach has been used to explore the parameter space and to isolate the variables that most affected the hit probability. In addition, parameters with no measurable effect on hit probability could be set to constant values so that simulation time would be spent exploring more-relevant variables. Modeled factors included laser spot size, scan patterns, linear scan speed, and overlap percentage required to meet the minimum detection limits.

4.2 Laser Power Module

The initial laser module incorporated a laser spot with uniform intensity. It was later rewritten to more realistically model an actual laser. Although previous methods of representing the laser were fast and provided early results, the ability of the module to represent actual systems or pass verification and validation (V&V) trials required a higher-fidelity method. Using output from a laser-profiling system, the new laser module can digitize the power at each individual pixel and then run an interpolation routine to scale the pixels of the profiler to the pixels that are needed in the model space. This allows the same beam profile to grow or shrink as needed. Finally, the module does a scanning pass over the interpolated beam shape to check for any negative pixels. Because it would not make sense to have negative energy, all negative pixels are set to zero. Figure 3 shows a comparison of the difference between the original laser spot on the left and the more-realistic laser spot on the right.

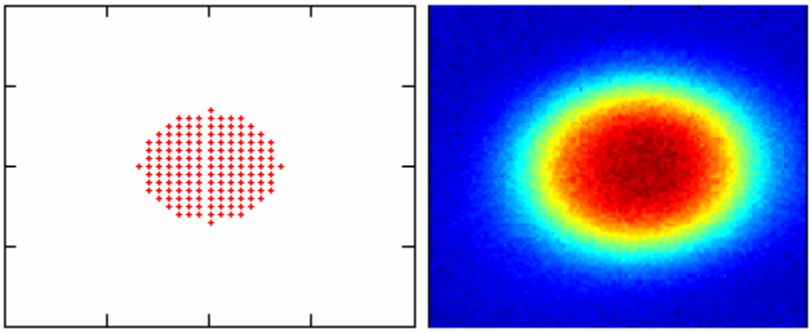

Figure 3. Old laser spot (left) vs new laser spot (right).

4.3 External Droplet-Import Module

To properly import droplet distributions from an external program such as VLSTRACK, a droplet-import module was written. This new module is used to take the outputs of a text file, such as the .rec files output by VLSTRACK for contaminant ground deposition, and create a droplet distribution. By using the normalized mass of contaminant deposited on the ground, a count of droplets of each size can be generated. Once this function has been described, the droplet-generation module can use selected sizes to create a witness card of arbitrary surface contaminant density.

4.4 Line-Scan Module

The initial spiral-scan pattern of the VLSTRACK model proved difficult to implement in the code of the V&V apparatus, which required a different scan pattern to be coded for the model. Like the spiral model, each pixel on this path is the center-point for a laser shot. For a scan shape, straight horizontal lines that went off of the paper were chosen. This shape allowed us to avoid the issue of modeling scanner slowdown during changes in direction. There can be an arbitrary number of passes, and scan speed and repetition rate both affect the density of

shots on each scan line. This approach was the quickest way to begin V&V testing and get results.

4.5 Droplet Thickness Parameter

In an effort to further generalize the model and keep it independent of detection technology, we needed to model droplet thickness for those technologies where penetration depth was a relevant factor. In the model, opacity is used to simulate thickness. This means that where droplets are modeled to be thin, those pixels are partially transparent, but progressively thicker pixels are modeled as more opaque. With an 8 bit data type, up to 255 levels of opacity can be used. With sufficient available memory or a small-enough witness card, 16 bits can be used for thickness. This would provide more than 65,000 thickness levels.

4.6 Test Results

The results for the calibration trials were good. The average difference between model and experimental results was about 10%, which was sufficient to validate the model within that test space. The results are shown in Section 5.5.

4.7 Possible Model Improvements

The model is used to determine whether surface contamination can be detected by calculating the energy returned to the detector when the surface is illuminated by a scanning laser. The model indicates that a detection event has occurred when the returned energy exceeds the detection threshold. Any properties or phenomena that can affect this process should be accounted for and modeled to provide accurate modeling results.

If the following four potentially important effects were included, the current model could be significantly improved: (1) Raman scattering, (2) surface properties, (3) beam angle effects, and (4) atmospheric attenuation. These properties can affect the processes by which UV laser energy propagates through the atmosphere to the surface, interacts with contaminants on the surface, and finally propagates through the atmosphere back to the detector.

Raman scattering is a phenomenon by which contaminants inelastically scatter the incident laser light. The spectrum of the scattered radiation is characteristic of the contaminant or the surface it impacts. If this latter energy has sufficient intensity and exceeds the detection threshold level, the surface contamination will be detected. Modeling this effect can be important to accurately determine the performance of a Raman-based detection system.

Because the contaminants reside on the substrate surface, surface properties can affect the manner and degree with which the incident laser energy interacts with the contaminants. A rough surface can be expected to produce results that differ from those of a smooth surface. Other potentially important surface properties to model include porosity and reflectivity.

The amount of surface contamination that the laser beam interacts with partially depends on the incident angle of the beam with respect to the surface. Incident angles close to perpendicular would be likely to interact with different amounts of contaminant when compared with incident angles that are close to parallel. Modeling this effect may have a significant impact on results. An analysis of the angle dependence of the Raman scattering return is part of the Standoff Raman for Surface Detection of Non-Volatile Threats project (CA09DET501C). The data and model from that effort can eventually be incorporated into the Surface Detection model.

Atmospheric absorption can have a significant effect on the energy levels that return to the detector, because the energy must propagate through the atmosphere on the trips between the surface and the detector. The atmospheric attenuation produced by this absorption is generally modeled using Beer's law. It can be important to include this effect when modeling detection systems operating over extended distances or near strong atmospheric absorption wavelengths.

Finally, we only recorded the raw hits that were output from our various models. Using a detection algorithm, we can apply some logic to these hit outputs and determine whether or not an alarm should be sounded. This would occur after some false-alarm data were obtained, but could be done entirely in post-processing of the data where there would be no need to repeat our processing with different detection algorithms. This scenario would operate more like real-world systems and provide a better model in those cases.

5. MODEL VALIDATION

5.1 Witness Card Printing

Data was gathered from 2-D witness cards using custom software developed by Hung Technology Solutions, LLC (Baltimore, MD). The software controls the positioning of the laser, digitization of the data, and output of information to the operator. To provide the highest levels of contrast, the witness cards used in these experiments consisted of black spots printed on white paper. To keep variability to a minimum, all witness cards were printed on a large plot printer provided by ITT Corporation (Edgewood, MD) using the same type of paper.

Two kinds of trials involving the 2-D witness cards were performed. The first was called the Calibration Trial and involved ordered rows of constant size droplets that were chosen to replicate a specific overlap value (Figure 4). The second trial was a Full-Witness Card Trial. These were run with a witness card that uses randomly selected droplets from an input distribution and assigns them random *x*–*y* coordinates on the card (Figure 5).

The second witness card used was created using the software package Matlab (MathWorks, Natick, MA). This witness card required data from an external source to generate a random distribution of droplets. To properly import droplet distributions from an external program such as VLSTRACK, a droplet-import module was written. This new module takes the outputs of a text file, such as the .rec files that are output by VLSTRACK for ground deposition and creates a droplet distribution. A droplet count for each size can be generated by examining

the normalized mass of contaminant that was deposited on the ground. Once this function has been described, the Droplet-Generation module can be used to select sizes and create a witness card of arbitrary surface density.

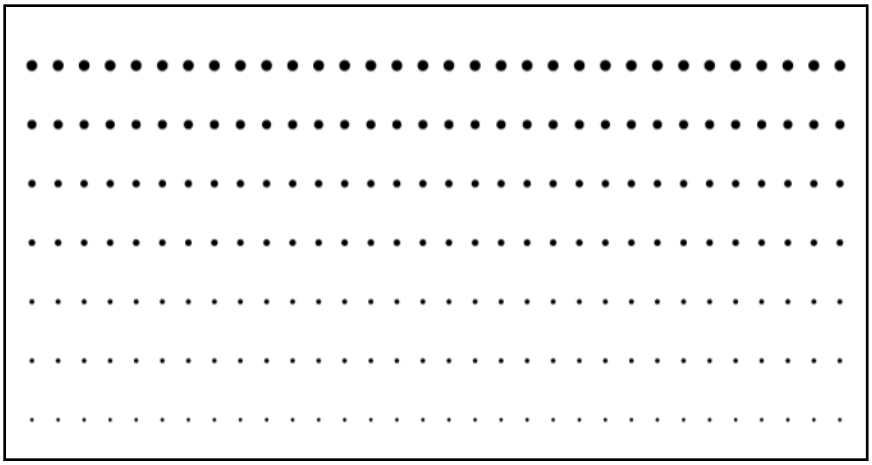

Figure 4. Sample calibration witness card.

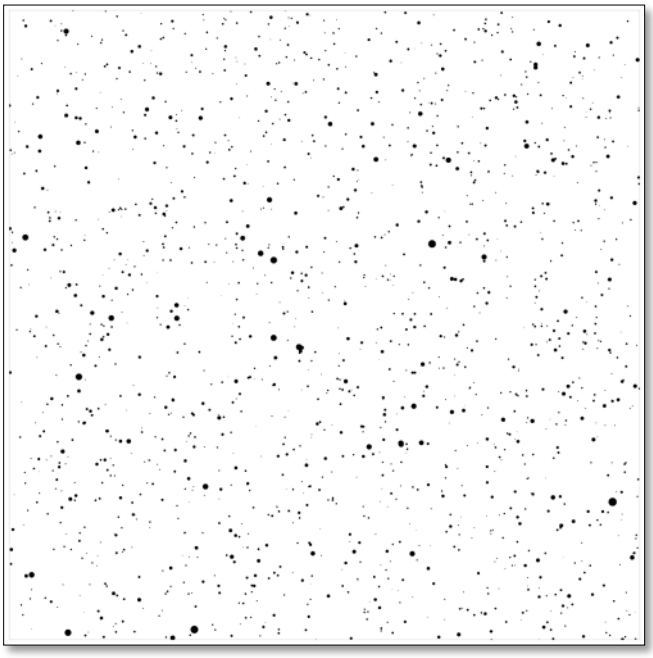

Figure 5. Witness card 15 generated from VLSTRACK data.

5.2 Detection Validation Software

Using Microsoft Visual C++ 6.0 software (Microsoft Corporation, Redmond, WA), a CFormView application was built from scratch to control the digitizer and gimbal and to record data. The software, named Surface Detect (Figure 6), uses the CFormView architecture for the benefits of the Document/View interface and to keep the simplicity of a simple dialog program. The CFormView is implemented on a single-document interface that allows only one instance of the view to run. Two pages have been added to the main view to add more space for the user interface. The first page consists of two oscilloscope displays. The top view shows the history of the laser pulses (shots) collected. Three lines advance from left to right. The red line represents the lowest value collected, and the green line represents the highest value recorded during a laser scan. The yellow line is the magnitude of the green line's value minus the red line's value. These three values are displayed in the upper-right corner of the page for easy reference. The range was set to 1000 laser pulses, and when that number is exceeded, the display resets back to the left. The last 200 points are saved and then redisplayed at the beginning of the scope. The current azimuth and elevation are shown at the lower-right corner of the page for quick reference. The lower oscilloscope depicts the entire number of samples collected during a test queue. This is provided to monitor the accuracy of each laser pulse and is used to set the acquisition time.

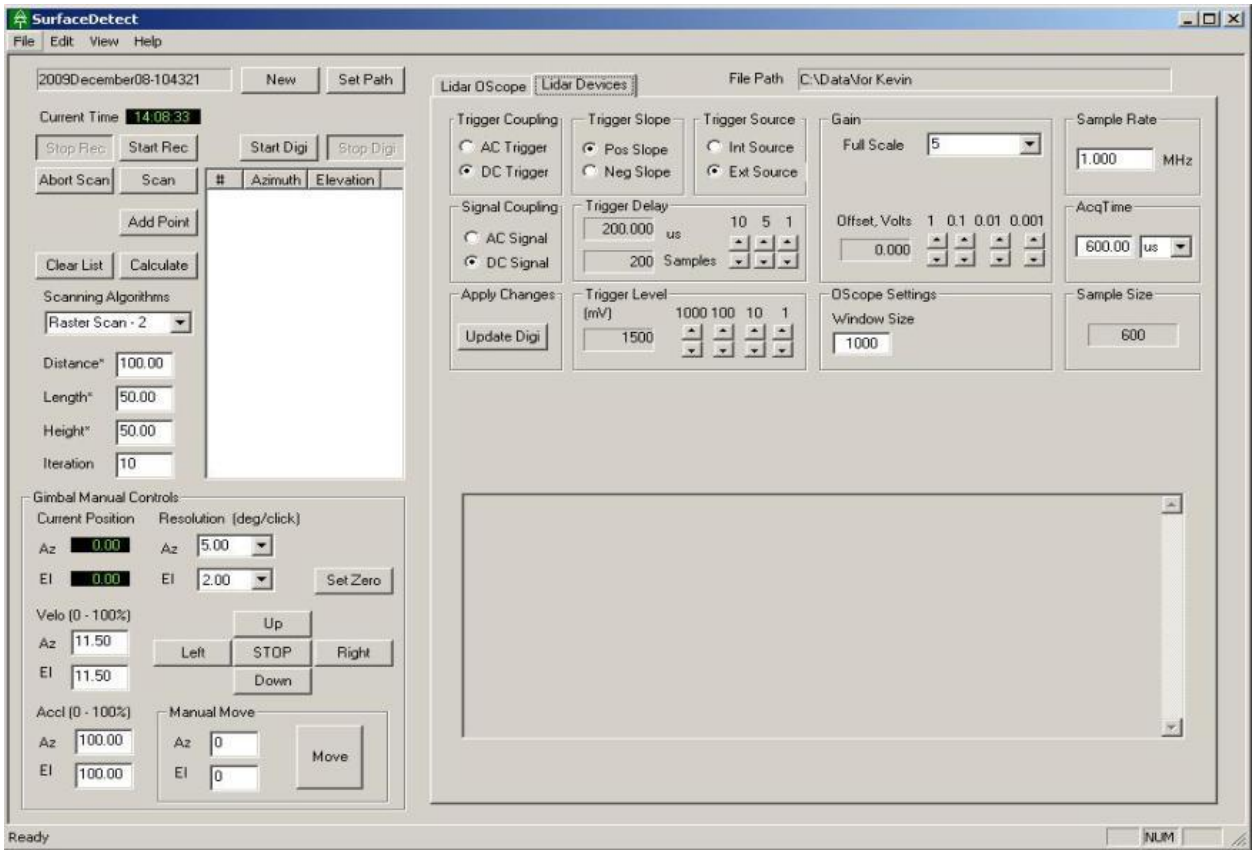

Figure 6. Surface Detect setting page.

5.2.1 File Recording

On the left side of the window are the main controls for this program. Starting from the top, the controls shown in Figure 6 are described as follows:

- The edit field, located on the top-left portion of the window, shows the current filename.
- The "New" file management button will automatically generate a new filename indicated in the Filename edit box. This filename will be used to label the recorded data files. The automatic filename is generated from the date and time when the New button is pressed.
- The "Set Path" file management button is used to change the file path where the files will be recorded.
- The "File Path" field, located on the top right portion of the window, shows the current path to the recorded files.
- The "Current Time" control, located on the top-left portion of the window, is a digital clock that is used to help the operator generate a new filename to include the time.
- The "Start Rec" button, located below the clock, is used to start recording a file.
- The "Stop Rec" button becomes available after the recording has started and can be used to halt the process.

The Surface Detect software records two files for each time a record operation is completed.

The first file is an American Standard Code for Information Interchange (ASCII) text file with a file extension of SDx. The SDx file provides the following information:

(1) Raw data filename,
(2) Number of samples per laser pulse,
(3) Full-scale voltage range,
(4) Gain,
(5) Offset voltage,
(6) Start time for the test, and
(7) Data. Each data line in the file contains:
    (a) Burst number,
    (b) Maximum voltage recorded in the burst,
    (c) Minimum voltage recorded in the burst,
    (d) Magnitude of the voltage (maximum voltage minus minimum voltage),
    (e) Azimuth position, and
    (f) Elevation position.

The second file contains the same information as the first file, but also records all samples from each laser pulse. This file will have a file extension of SDD. To save space, this data is recorded in binary format and must be played back using the Recorded Data application or using analytical software such as Matlab.

5.2.2 Data Collection

Clicking on the "Start Digi" button (Figure 6) starts the Acqiris digitizer, and clicking on the "Stop Digi" button stops the digitizer. The flow chart (Figure 7) shows the algorithm used to collect data during this process. When the operator clicks the "Start Digi" button, the Surface Detect software has a dedicated thread to handle data acquisition. The thread contains a data collection loop that will run until the operator stops the acquisition. In the data collection loop, the digitizer is armed and holds until there is an external TTL (transistor-transistor logic) signal (external trigger) sent from the laser. A timeout of 2 s is set for each holding period. If no trigger is received within 2 s, an error message is posted on the Devices Page message board.

When an external trigger arrives, the digitizer collects data for 200 μs. The software extracts the data from the digitizer's memory and copies it to a buffer that is supplied by the software. This buffer formats the information into a local data structure for packaging. An algorithm is used to determine whether or not data is currently being recorded. If data is recording, the data will be placed in a queue to be written to a file. The final step in the loop places the data into a display queue to render the oscilloscope displays (Figure 8).

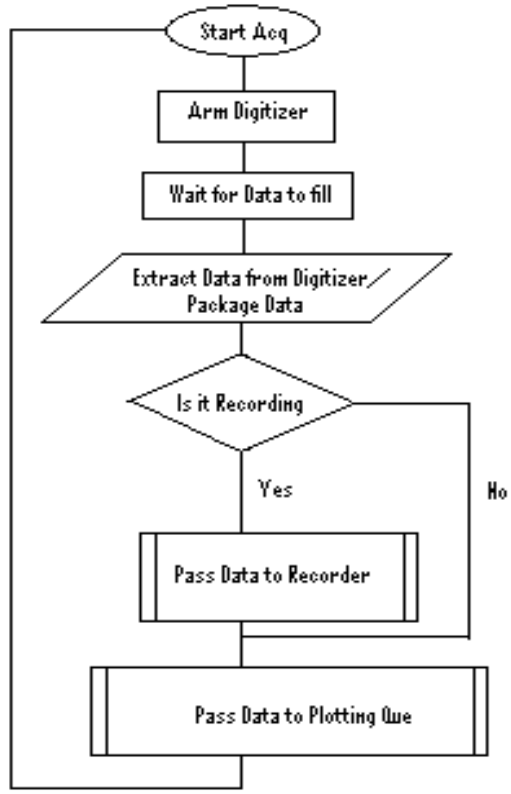

Figure 7. Design algorithm for the Surface Detect application.

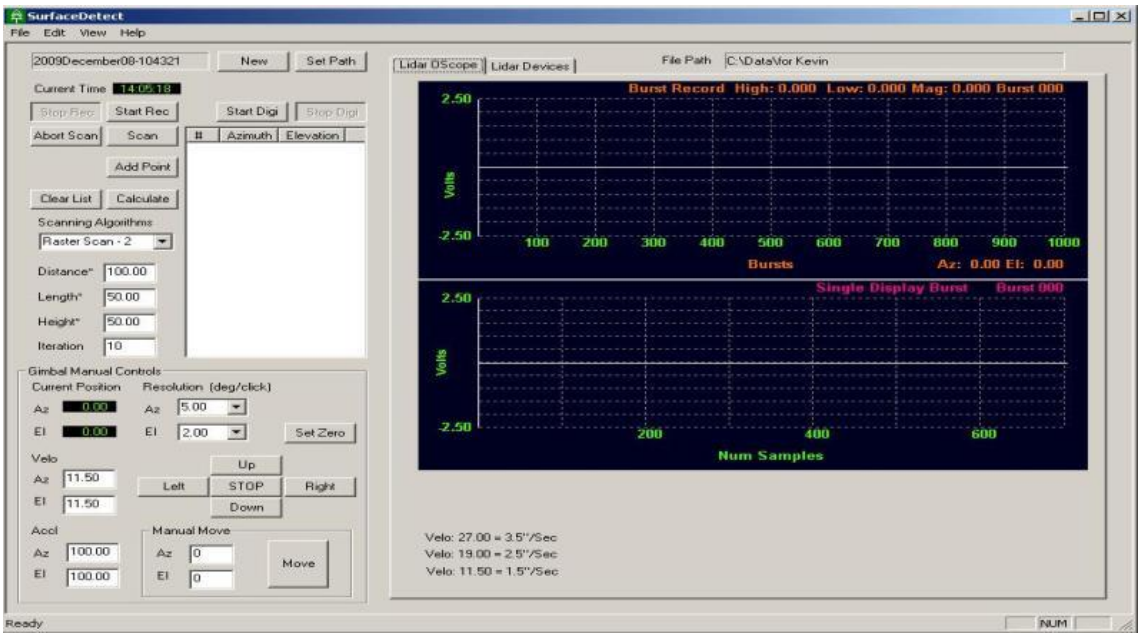

Figure 8. Surface Detect application showing the oscilloscope display.

5.3 V&V

The UV diode laser-based laboratory instrument (Figure 9) was developed to provide intercept statistics for different scan patterns and speeds. A 0.5 × 0.5 m witness card, with a known droplet distribution, was used to validate the scanning model. The experimental intercept statistic results were compared to the modeling data from the same target. A calibration witness card (Dugway Sprayer witness card at 0.5 g/m^2 of contaminant) and a VLSTRACK output witness card at 0.5 g/m^2 of contaminant were scanned for the validation experiment and compared with the scan model predictions. The Dugway Sprayer witness card was generated using from actual sprayer droplet data and was not obtained through VLSTRACK modeling. Parameters considered in the validation experiment were percent overlap, laser repetition rate, linear scan speed, and scan pattern. A laser beam intercept was defined as an optical return that was reduced in signal amplitude to 70 or 85% for 30 or 15% overlaps, respectively, or less when compared with the white background.

Figure 9. V&V setup.

A Direct Jet 1309 printer (Direct Color Systems, Rocky Hill, CT) was used to simulate the deposition of modeled droplet distribution on relevant surfaces with actual chemicals. This unique printer is a flatbed inkjet printer that can be used to deposit chemical simulants on a variety of substrates including Teflon, plastic, wood, metal, stone, and glass materials. The printer can deposit a known mass of chemical simulants on a 6 in. square surface using a portion of the VLSTRACK output. This surface can then be used for performance testing

of instruments against known chemical materials, mass, distributions and surface backgrounds. Moon et al.[3] provide a detailed description of the Direct Jet 1309 printer.

5.3.1 Scan Model Validation Experiment Setup

The original laser (Micro Laser Systems [Garden Grove, CA] model L4405M-48BTE) was replaced with a Coherent Cube laser (Coherent, Inc.; Santa Clara, CA). The new laser maintains a more-stable output power and beam shape. The shape of the beam generated by the Micro Laser Systems laser (Figure 10, left) is more of an oval and less defined when compared with the more-defined and rounded shape of the laser generated by the Coherent Cube system (Figure 10, right). The Coherent Cube is a 405 nm laser and has greater range of beam control via a universal serial bus (USB) interface from the acquisition computer. The software with the Coherent Cube laser allows the operator to precisely change the power levels, as compared with the less-reliable manual (small screwdriver) method used by the Micro Laser Systems unit.

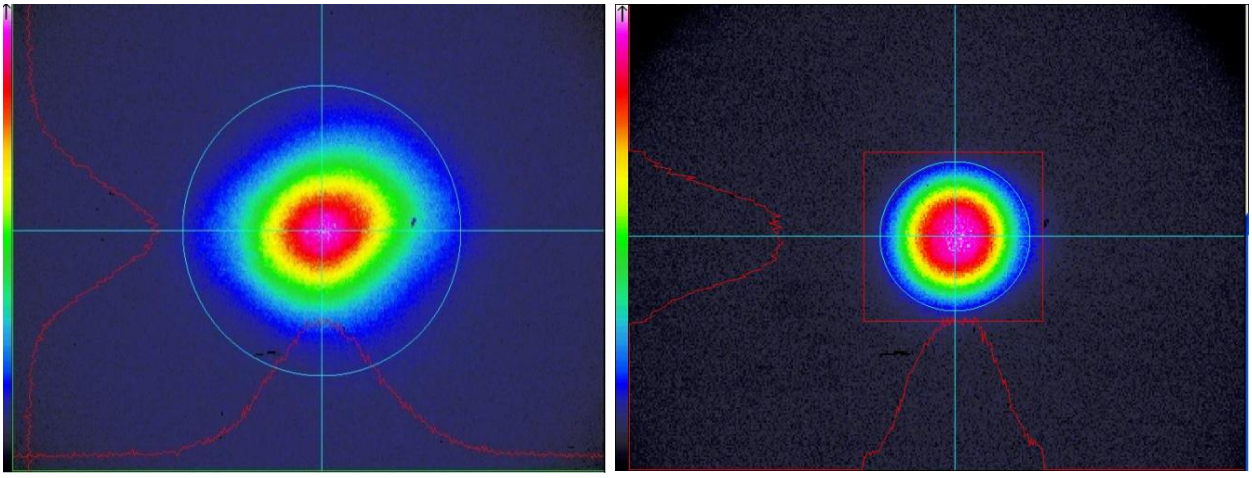

Figure 10. Beam profiles of Micro Laser Systems L44M-48BTE laser (left) and Coherent Cube laser (right).

The original Micro Laser Systems laser did not maintain constant power for a prolonged period. Test results showed that were was up to 10% loss in power when this laser was used for more than 5 h. The signal return from the white spectra levels at the later portion of the experiment dropped close to 30%, which approached the detection threshold that was defined at the beginning of the experiment.

In addition to replacing the laser, redesigning the laser setup was needed. The original design included an iris to control the laser beam size. Using an iris created unwanted scatter from the edge, resulting in a halo effect at the target. To reduce the halo effect, a small pinhole was placed between two lenses. These changes resulted in a more-defined beam shape as shown in Figure 11. The second lens on the setup also allows the operator to change the diameter of the beam. The average diameter for the beam using the Coherent Cube laser is about 1.8 mm.

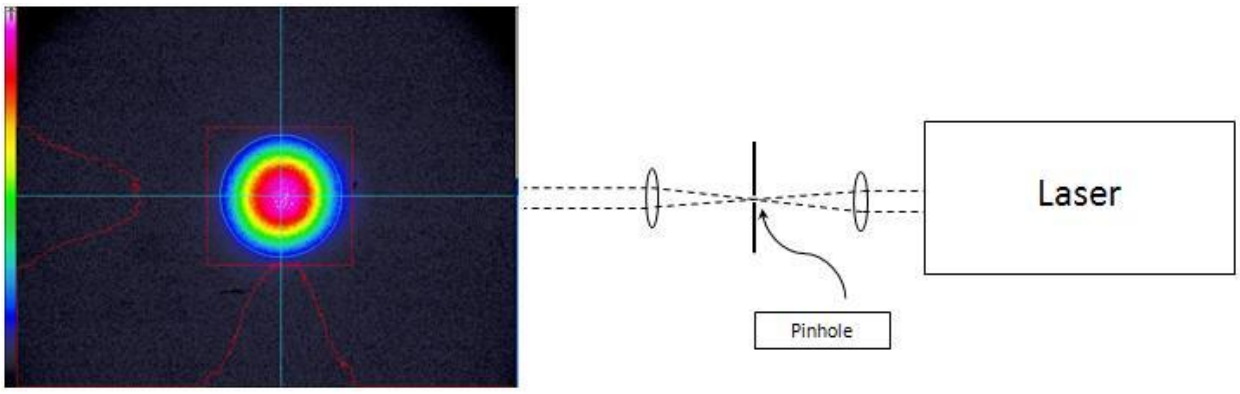

Figure 11. Laser setup with pinhole and optics.

A Hewlett-Packard (Palo Alto, CA) pulse generator was used as an external trigger source for the Coherent Cube laser, and the laser pulse width was set to 1 ms for each laser pulse. The repetition rate for the laser is variable depending on the test. Repetition rates range from 10 to 250 Hz.

A backstop was used to mount the witness cards for data collection. A mounting frame, consisting of a wooden square with a 0.5 × 0.5 m opening in the center (Figure 12), was added to the backstop to help position the witness cards. The edge of the wooden frame was wrapped in a black felt material to absorb any laser energy. Two mounting frames were made, one for use with the witness card and another for use with the white calibration paper. The witness card was taped to the mounting frame using two-sided tape, and the mounting frame was attached to a 90° bracket by a single woodscrew. To aid in height adjustments, the bracket was attached to a rack-and-pinion shaft that was attached to the optics table. Two C-clamps were used to secure the frame to the backstop. The use of the single woodscrew allowed the witness card to rotate so that it could be made level with the scan track. Once the witness card was level, the bulk of the frame was supported by the two C-clamps. To change the height of the witness card, we removed the C-clamps and twisted the knob on the rack. The C-clamps were reapplied when the desired height was set.

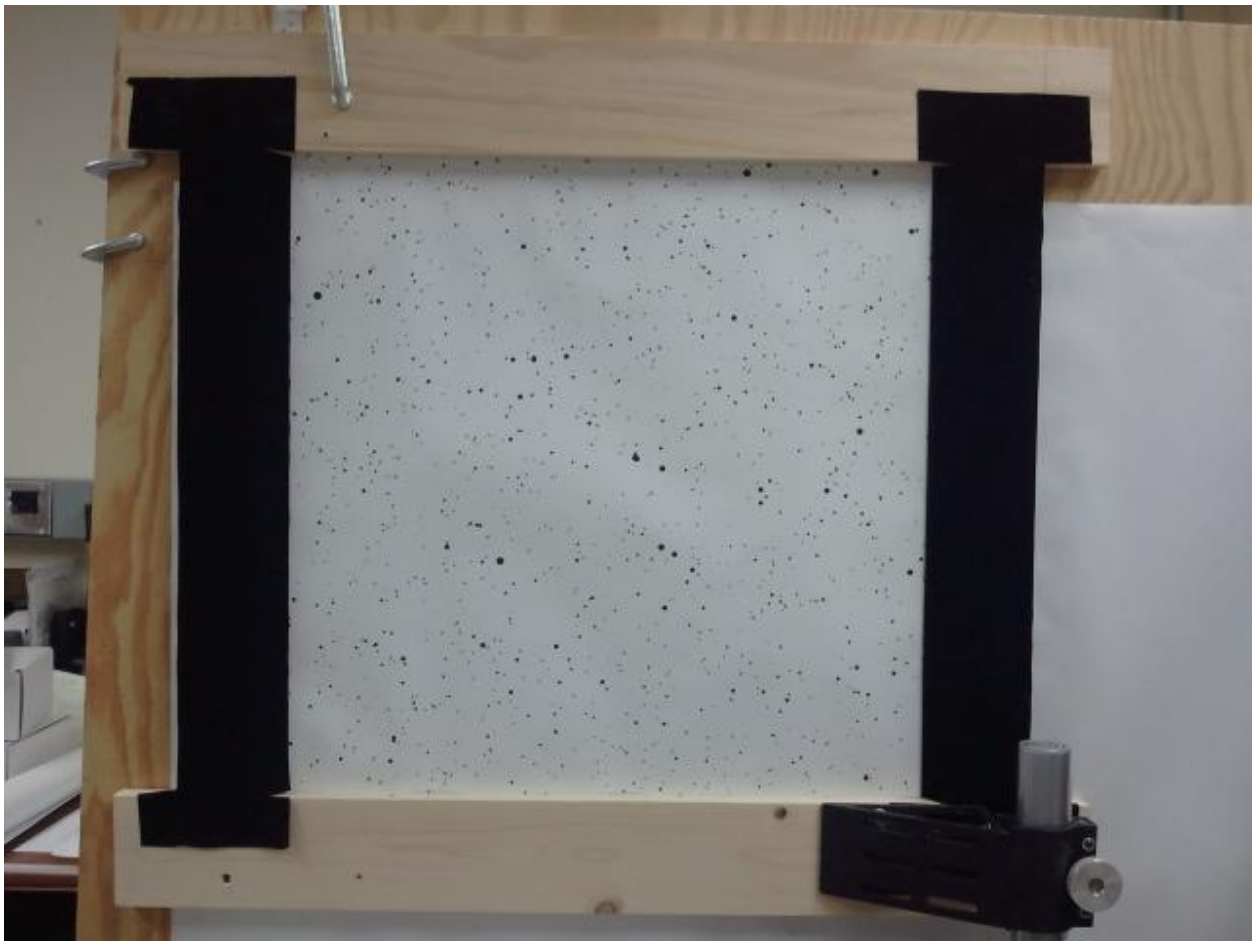

Figure 12. VLSTRACK witness card 15 on mounting frame.

5.3.2 Data Collection Procedure

The data collection procedure consisted of using a laser scan on a witness card with the following parameters:

- Repetition rate at 10, 25, 100, or 250 Hz;
- Beam diameter of ~1.8 mm at 98%;
- Three scan speeds of 1.5, 2.5, and 3.5 in./s;
- Scan passes that can vary from 5 to 10, depending on the experiment; and
- Starting point of witness card, which was discussed and agreed upon before the test.

The laser was scanned from left to right and back again to make predetermined raster scan passes. The data collected was post-processed with a Microsoft Excel script to compute the results. The results were averaged and compared with the model's performance. To ensure the same beam size and shape, all data was collected during the same day.

5.3.3 System Calibration

Initially, the white paper background and black ink that would be used to create a witness card were scanned to determine the signal contrast ratio. Figure 13 shows the white paper to black ink contrast of approximately 45 to 1. Following the determination of a contrast ratio, a calibration witness card was created (Figure 14, which is the same as Figure 4 that was reproduced here for convenience). The calibration card was made up of seven rows of droplets with varying droplet sizes. From the bottom to the top of the card, the droplet diameters were 1.2, 1.5, 1.6, 2.1, 2.6, 3, and 3.5 mm. Each row was scanned once, from left to right, with scan speeds of 1.5, 2.5, and 3.5 in./s. These results were compared with modeling results.

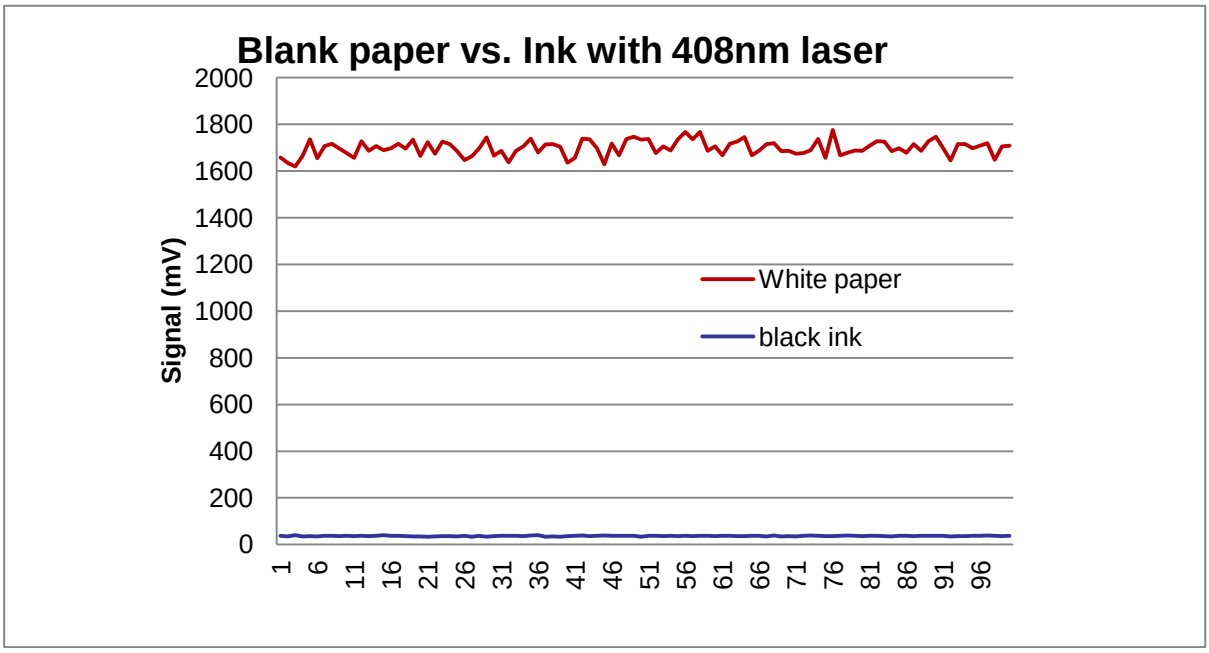

Figure 13. White paper background and black ink laser-scanning results.

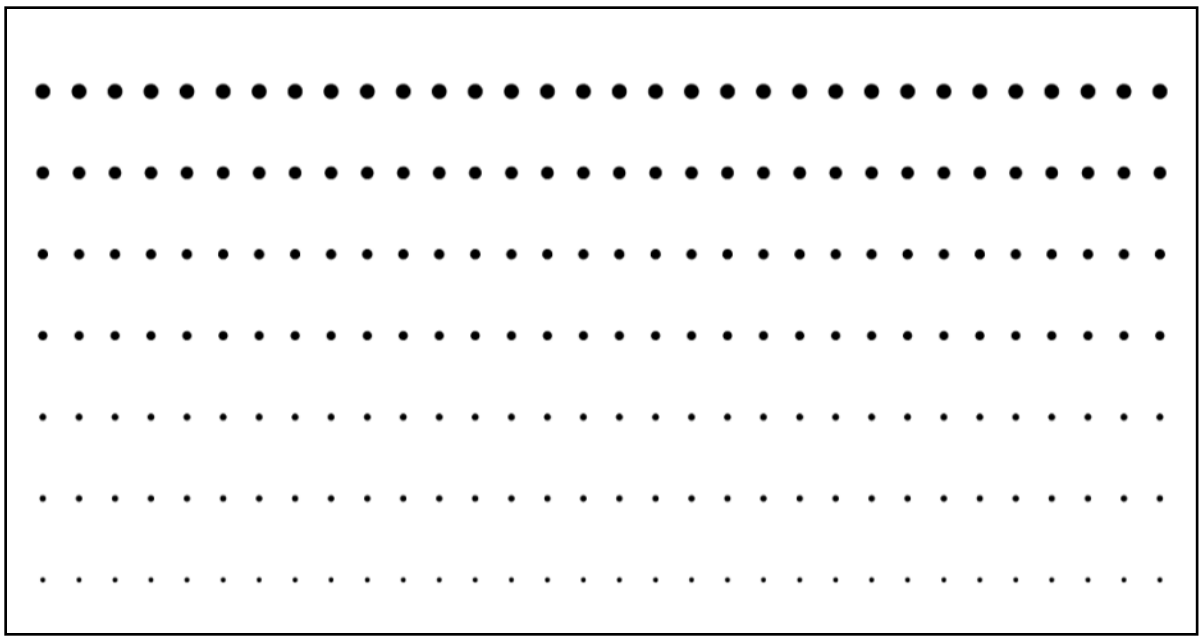

Figure 14. Calibration witness card.

5.3.4 Data Analysis

Three calibration files were collected before and after the laser-scanning trials. These files were: (i) scanning of paper background, (ii) scanning of black ink, and (iii) focusing on a spot that was slightly larger than the beam size. The information from these calibration files helped to compensate for a signal that was returned by sources other than the laser beam itself (such as the halo).

By subtracting the average of black ink ($Black_{Avg}$) and the average of black spot $(Black\_w/halo)_{Avg}$, we can determine the offset produced by the halo

$$Halo_{offset} = Black_{Avg} - (Black\_w/halo)_{Avg} \quad (1)$$

Gimbal positions of left and right edges of the test card were recorded to be used for providing a data range. Data points collected outside these boundaries were not used during data processing. High ($High_{avg}$) and low (Low_{avg}) averages were calculated by using top and bottom 5% of the data range, respectively. Subsequently, the detection threshold can be determined as follows:

$$Threshold = (High_{avg} - Black_{avg}) \times 0.7 + Halo_{offset} \quad (2)$$

Once the detection threshold was determined, the trial data set was passed through a series of filters. By counting the number of laser pulses within the boundaries and the number of laser pulses that met the detection threshold, we determined the percentage of detections per laser pulse (hits per shot) (Figure 15). The hits per shot are equal to the number of laser pulses that produced a signal below the threshold, per number of laser pulses within the boundaries.

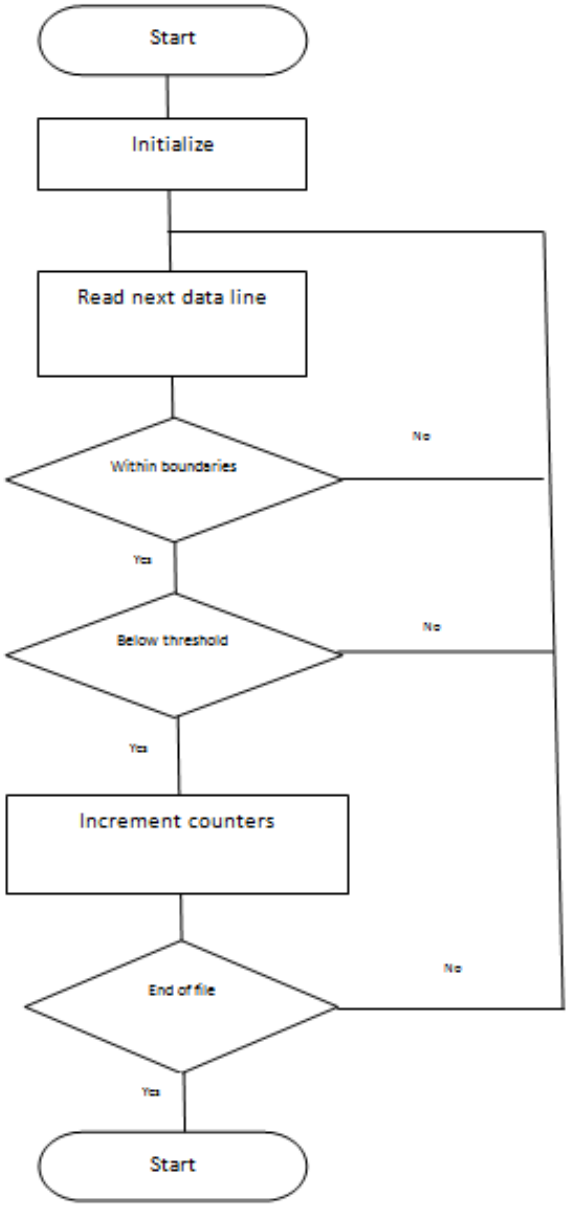

Figure 15. Design algorithm.

5.4 Initial Calibration Card Results

Table 1 contains the initial experimental results compared to the software modeling results. The laser-scanned data were normalized to hits per shot. There was strong correlation with droplet sizes. Overall, the results showed good repeatability and matched well with the software modeling results. Details of the scan model procedure and results are provided in Appendix A.

Table 1. Results from Calibration Witness Card

PARAMETERS						MODEL RESULTS			EXPERIMENT RESULTS		
Spot Size	Scan Speed	Overlap (%)	Rep Rate	Scan Pattern	Drop Size (mm)	# Shots	# Hits	Hits/Shot	# Shots	# Hits	Hits/Shot
3.2	1.5	30	25	Line	3.5	185	87	47.03%	180	82	45.47%
3.2	2.5	30	25	Line	3.5	111	54	48.65%	110	50	45.43%
3.2	3.5	30	25	Line	3.5	80	37	46.25%	77	33	42.46%
3.2	1.5	30	25	Line	3	185	72	38.92%	179	71	39.49%
3.2	2.5	30	25	Line	3	111	48	43.24%	108	44	40.42%
3.2	3.5	30	25	Line	3	80	30	37.50%	75	29	38.05%
3.2	1.5	30	25	Line	2.6	185	60	32.43%	179	62	34.82%
3.2	2.5	30	25	Line	2.6	111	32	28.83%	108	37	34.37%
3.2	3.5	30	25	Line	2.6	80	26	32.50%	78	27	34.06%
3.2	1.5	30	25	Line	2.1	185	51	27.57%	179	51	28.48%
3.2	2.5	30	25	Line	2.1	111	32	28.83%	110	30	27.65%
3.2	3.5	30	25	Line	2.1	80	22	27.50%	75	20	26.57%

5.5 Data Collection from VLSTRACK Witness Card

The laser-based experiment was set up to scan a witness card pattern consisting of black simulated droplets on a white background. The optical detector measured the signal return from white and black areas. Intercepts were defined as return signals that were ≤30% of the white background signal return.

The first step in collecting data was to measure the size of the beam. The Coherent Beam View Analyzer software (Coherent, Inc.) provides a large set of information about the beam; however, only the diameter of the beam was needed. The laser energy was measured using Laser Cam IIID (Coherent, Inc.), which is a laser beam profiler. The diameter of the beam was measured at the 86.5% intensity location and then estimated at 98% for use with the model (Figure 16). This information was then used in the modeling experiments. In addition to the visual image of the beam, an ASCII image (IMG) file was generated. The ASCII image is a pixilated version of the visual image. Each pixel contains an 8-bit weighted ASCII numerical value representing the power level in the field of view of the camera. Because the laser's behavior varies each time it is turned on, the matrix of data that was used to build a model of the beam fired was only valid for that day. The image and ASCII data were collected before each experiment.

Another method to determine the beam size was to calculate the beam width using experimental data applied to a Gaussian equation

$$P = P_0\left[1 - e^{-\frac{2d^2}{\omega^2}}\right] = 2.26\ \text{mm} \tag{3}$$

where

P_0 is total beam power;
P is power passing through a circle of diameter (d); and
ω is beam diameter at the 86.5% power point.

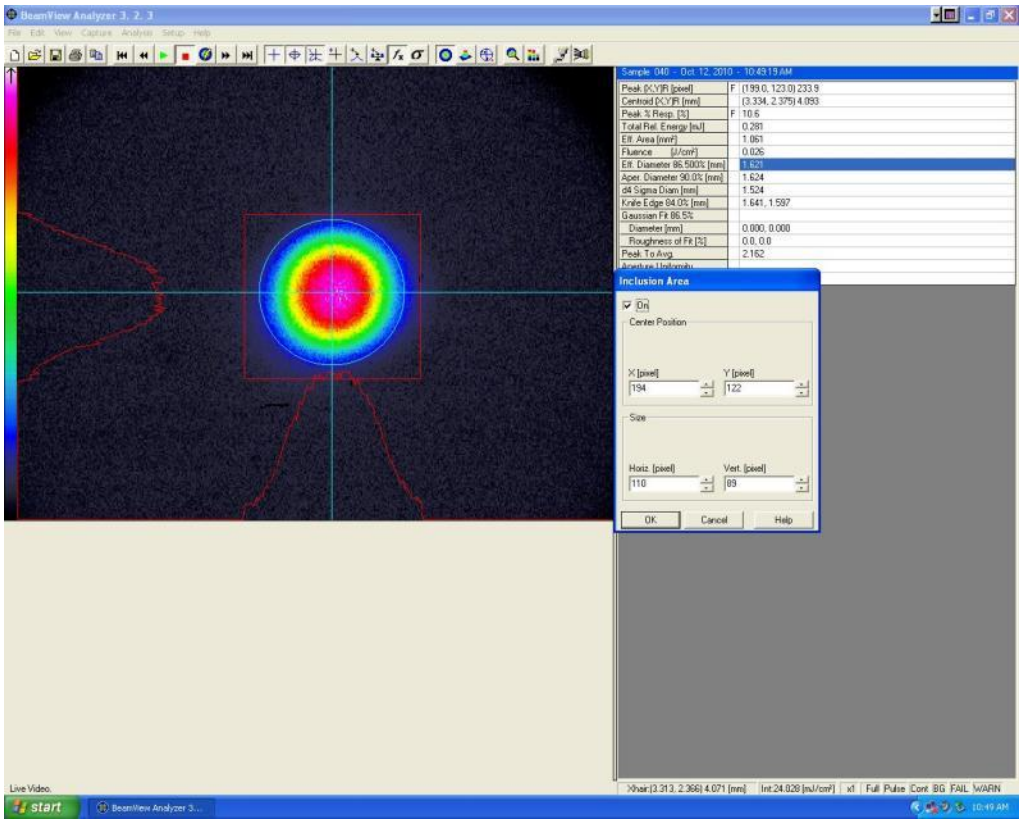

Figure 16. Beam View Analyzer application showing a typical laser beam profile.

The output voltage from a 50% area black spot calculated using the Gaussian equation was 479 mV, and the detector voltage measured from a 50% area spot was 494 mV (3% error). The actual data collection process started with programming a scan pattern for the gimbal. The scan pattern is usually determined by the type of witness card. Calibration witness cards involve a simple left-to-right scan for each line of dots. VLSTRACK and sprayer witness cards involve a raster scan pattern; however, only the horizontal passes from the raster scan are used (Figure 17). The raster scan for the VLSTRACK and sprayer cards have their boundaries set outside of the witness card so that the laser can cross into the mounting frame's energy-absorbing materials. The energy-absorbing material creates low-level zones that mark the starting and stopping points of a pass. The starting and stopping points are in the outer edges of these low-level zones, where the elevation changes and acceleration and deceleration occur. This change in position and speed allows the gimbal to accelerate or decelerate outside the field of interest, ensuring a constant scan speed for the inside of the witness card.

White levels were recorded to provide background subtraction for the experimental data. The path scanned from the white paper matches the experiment's path. This provided a same-shot subtraction for each data point. The threshold was calculated for each point by taking the white level and then multiplying the point by 70 or 85% for 30 or 15% overlaps, respectively. Any data points within the left and right edges of the witness card were considered valid data points.

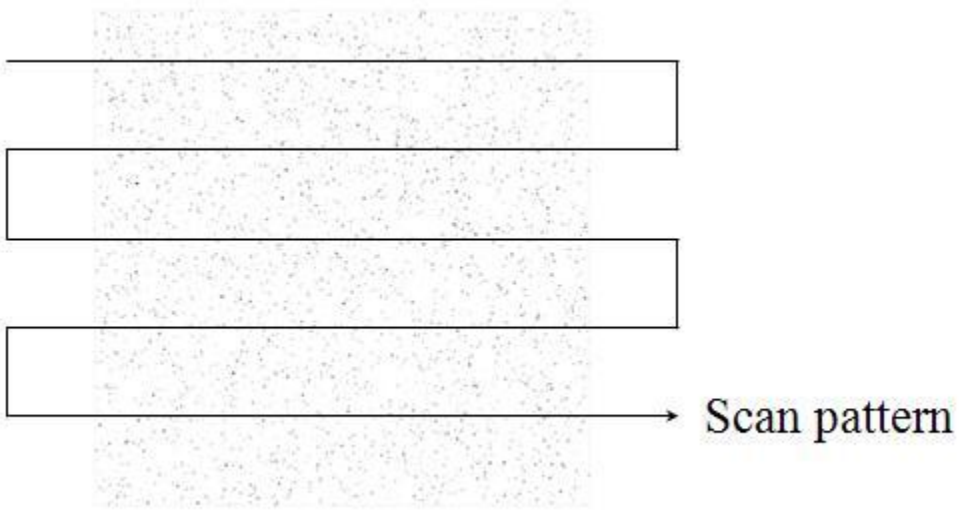

Figure 17. Five-pass raster scan pattern.

The procedure for collecting data with the witness card was the same as for collecting the white background. Great care was taken to ensure the witness card mount was positioned in the same area as the white background mount. A hit is defined as a signal returned from the detector that is 30% less than the average of the white background return.

One of the problems with scanning across a large range is the inability to have the beam travel in a straight line. When the laser is firing on a large angle, the path of the beam will arc up or down depending on the angle. Higher positive angles will cause an upward arc, and negative angles will have a lower arc. This creates difficulties when scanning small spots in the calibration witness card. To minimize this effect when collecting data on calibration witness cards, the experiment limited the elevations used to ±7°. To cover the entire witness card, the mount was raised and lowered as needed for each line. This problem was not as prevalent when testing sprayed witness cards because of the random placements of the dots on the witness card.

5.5.1 Data Processing

To compare the model's performance with the experiment, a Microsoft Excel script was created to process the data. Creation of the Excel spreadsheet required that the left and right scan limits of the witness card be used to determine the field-of-view. During execution of the script to create the sheet, the white data was imported and the valid points in the field-of-view were extracted out. This was determined by the width of the frame and the size of the witness card. The field-of-view was biased slightly to the left by the way the witness card was

mounted in relationship to the laser. The raw data from the witness card experiment was imported into the Excel script and processed in the same fashion.

5.5.2 Witness Card Results

Calibration, Dugway Sprayer, and VLSTRACK witness cards results are shown in Tables 2–5. The results shown are for scan speeds of 1.5, 2.5, and 3.5 m/s; repetition rates of 10, 25, 100, and 250 Hz; and overlap thresholds of 15 and 30%.

Table 2. Results for Calibration Witness Card

Parameters					**Experiment Totals**			**Model Totals**			
Laser Spot Size (mm)	Scan Speed (inch/second)	Overlap (%)	Rep rate (Hz)	Scan Pattern	Shots	Hits	Hits/Shot	Shots	Hits	Hits/Shot	Difference
2.26	1.5	30	25	Line - 150%	498	84	16.9%	501	75	15.0%	-1.9%
2.26	1.5	30	25	Line - 100%	488	70	14.3%	501	60	12.0%	-2.4%
2.26	1.5	30	25	Line - 75%	485	57	11.8%	501	60	12.0%	0.2%
2.26	1.5	30	25	Line - 50%	491	25	5.1%	501	30	6.0%	0.9%
2.26	1.5	30	25	Line - 35%	423	10	2.4%	501	0	0.0%	-2.4%
2.26	1.5	30	25	Line - 25%	492	0	0.0%	501	0	0.0%	0.0%
2.26	1.5	30	25	Line - 15%	488	0	0.0%	501	0	0.0%	0.0%
2.26	2.5	30	25	Line - 150%	282	47	16.7%	300	60	20.0%	3.3%
2.26	2.5	30	25	Line - 100%	283	38	13.4%	300	30	10.0%	-3.4%
2.26	2.5	30	25	Line - 75%	281	33	11.7%	300	30	10.0%	-1.7%
2.26	2.5	30	25	Line - 50%	284	19	6.7%	300	30	10.0%	3.3%
2.26	2.5	30	25	Line - 35%	283	5	1.8%	300	0	0.0%	-1.8%
2.26	2.5	30	25	Line - 25%	288	0	0.0%	300	0	0.0%	0.0%
2.26	2.5	30	25	Line - 15%	256	0	0.0%	300	0	0.0%	0.0%
2.26	3.5	30	25	Line - 150%	198	31	15.7%	216	36	16.7%	1.0%
2.26	3.5	30	25	Line - 100%	195	29	14.9%	216	29	13.4%	-1.4%
2.26	3.5	30	25	Line - 75%	208	21	10.1%	216	23	10.6%	0.6%
2.26	3.5	30	25	Line - 50%	220	12	5.5%	216	17	7.9%	2.4%
2.26	3.5	30	25	Line - 35%	199	3	1.5%	216	0	0.0%	-1.5%
2.26	3.5	30	25	Line - 25%	194	0	0.0%	216	0	0.0%	0.0%
2.26	3.5	30	25	Line - 15%	202	0	0.0%	216	0	0.0%	0.0%

Table 3. Results for Dugway Sprayer Witness Card

	Parameters					Model Results			Experiment Results		
	Spot Size (mm)	Scan Speed (inch/second)	Overlap (%)	Rep rate (Hz)	Scan Pattern	Shots	Hits	Hits/Shot	Shots	Hits	Hits/Shot
Trial 1	2.9	1.5	15	25	5-pass raster	1650	22	1.33%	1624	20	1.23%
	2.9	2.5	15	25	5-pass raster	990	15	1.52%	937	28	2.99%
	2.9	3.5	15	25	5-pass raster	710	10	1.41%	664	11	1.66%
Trial 2	2.9	1.5	15	25	5-pass raster	1650	29	1.76%	1607	28	1.74%
	2.9	2.5	15	25	5-pass raster	990	22	2.22%	931	13	1.40%
	2.9	3.5	15	25	5-pass raster	710	10	1.41%	650	11	1.69%
Trial 3	2.9	1.5	15	25	5-pass raster	1650	16	0.97%	1541	25	1.62%
	2.9	2.5	15	25	5-pass raster	990	6	0.61%	937	13	1.39%
	2.9	3.5	15	25	5-pass raster	710	4	0.56%	650	11	1.69%

Table 4. Results for Dugway Sprayer Witness Card No. 2

Parameters					Model Results					Experiment Totals			
Laser Spot Size (mm)	Scan Speed (inch/second)	Overlap (%)	Rep rate (Hz)	Scan Pattern	Shots	Hits 1	Hits 2	Hits 3	Hits/Shot	Shots	Hits	Hits/Shot	Hits/Shot Difference
2.482	1.5	15	10	5 lines	660	15	19	10	2.2%	643	12	1.9%	0.3%
2.482	1.5	30	10	5 lines	660	4	3	4	0.6%	643	2	0.3%	0.3%
2.482	2.5	15	10	5 lines	395	5	9	6	1.7%	368	7	1.9%	-0.2%
2.482	2.5	30	10	5 lines	395	3	4	4	0.9%	368	0	0.0%	0.9%
2.482	3.5	15	10	5 lines	285	9	4	3	1.9%	255	5	2.1%	-0.2%
2.482	3.5	30	10	5 lines	285	2	0	1	0.4%	255	2	0.9%	-0.5%
2.482	1.5	15	25	5 lines	1645	29	37	39	2.1%	1594	34	2.1%	0.0%
2.482	1.5	30	25	5 lines	1645	14	12	11	0.7%	1594	5	0.3%	0.4%
2.482	2.5	15	25	5 lines	985	17	24	18	2.0%	913	24	2.6%	-0.6%
2.482	2.5	30	25	5 lines	985	7	7	6	0.7%	913	4	0.4%	0.3%
2.482	3.5	15	25	5 lines	705	19	11	14	2.1%	655	11	1.7%	0.4%
2.482	3.5	30	25	5 lines	705	6	3	8	0.8%	655	1	0.2%	0.7%

The agreement between the experimental and scan model results was generally very good, with an overall difference of >3.5%. This confirmed the scan model's ability to predict detection probabilities (hit rates) based on a knowledge of the sensor scan speed, laser repetition rate, and overall sensor sensitivity as captured by the minimum overlap (in percent) required for droplet detection.

Table 5. Results from the VLSTRACK Witness Card

				30% Overlap		15% Overlap	
Rep Rate	Speed	Line #	Shots	Hits	Hits/Shot	Hits	Hits/Shot
10Hz	1.5"/s	Raster	666	29	4.35%	31	4.65%
	2.5"/s	Raster	375	12	3.20%	14	3.73%
	3.5"/s	Raster	268	11	4.10%	12	4.48%
250Hz	1.5"/s	Raster	15750	598	3.80%	573	3.64%
	2.5"/s	Raster	9100	185	2.03%	231	2.54%
	3.5"/s	Raster	6500	216	3.32%	252	3.88%

6. MODELING A PASSIVE-IMAGING SYSTEM

The passive-imaging system was used to determine the percentage of coverage on a surface. To compare the modeling of a passive-imaging system, Witness Card 15 was created with a resolution of 11800 × 11800 pixels to simulate a surface area of 0.5 × 0.5 m. Witness Card 15 was based on data from VLSTRACK with a mass loading of 0.5 g/m^2. To compare results, researchers used a validation system with a digital camera to capture a bitmap of the witness card with a resolution of 2040 × 2040 pixels. Witness Card 15 was loaded into the modeling system memory, and the resolution was downgraded to 2040 × 2040 pixels to match the settings used in the validation system. Then post-processing was performed with each system using their unique algorithms to determine the percentage of coverage (Figure 18).

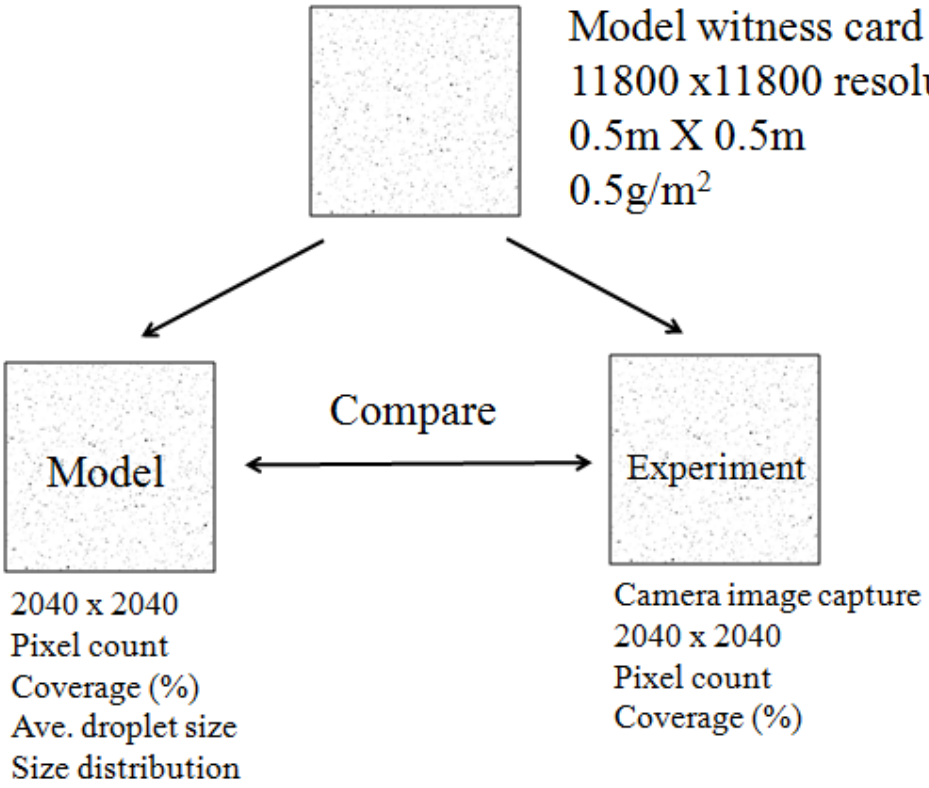

Figure 18. Modeling and validation for passive imaging.

6.1 Validation Setup

The camera used to capture images for the validation was the Allied Vision Technologies (Stradtroda, Germany) GE2040 model. This camera came with a software development kit (SDK) that can be used to build applications for controlling the camera. Communication between the control computer and the camera is accomplished using a gigabit ethernet connection. However, the development software, Microsoft Visual C++ 6.0, used in this experiment, was not compatible with the SDK provided by Allied Vision Technologies, and a newer version of the SDK was not available. Therefore, the software provided by Allied Vision Technologies was used instead. The camera was mounted on the gimbal, and the images captured were downloaded into the control computer.

An application was developed to process the images captured. The CBitmapTest application was developed to count pixels and identify spots based on contrasting colors (Figure 19). CBitmapTest can be used to count the number of pixels that are darker than a predetermined threshold. These dark pixels are stored in a vector for post-processing. Dark pixels located on the edge of a spot are added to another vector. These edge pixels are further refined to form a spot. The algorithm progresses along the edge of the dark pixels until it comes back to the origin. When this has completed, a new spot will have been discovered. The

implementation at the time of this report was not very efficient, and more work would be required to get this algorithm to a usable state.

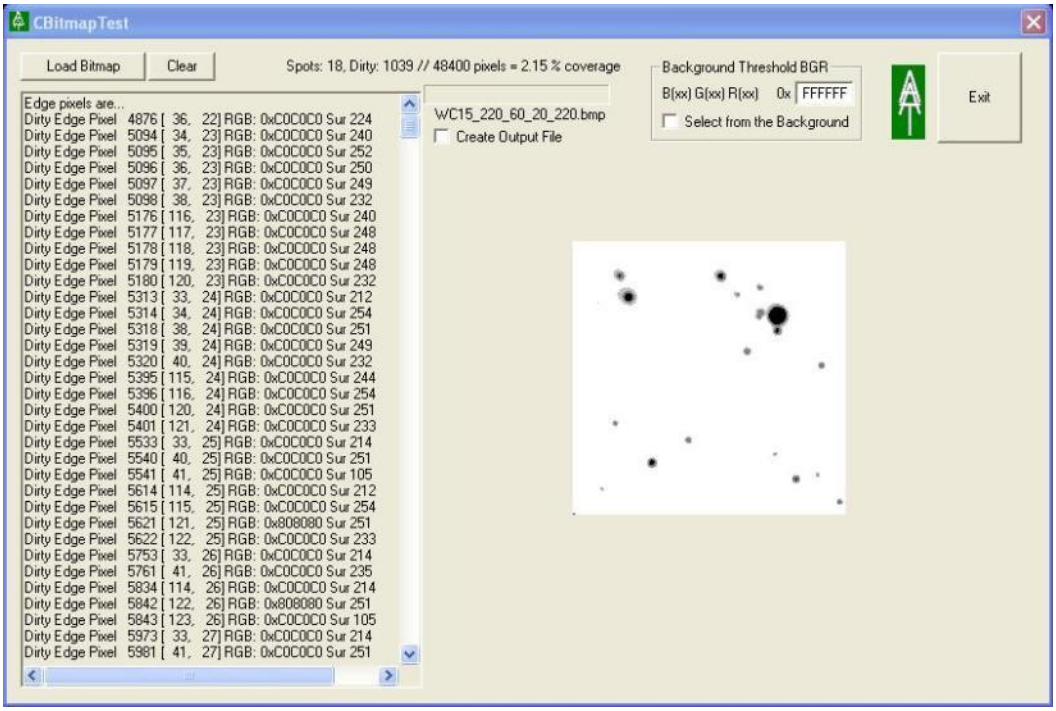

Figure 19. CBitmap application.

In an effort to make the application more user-friendly, the option to select the background threshold from the image has been provided (Figure 20). The original method used to input a threshold required the operator to know the RGB (red, green, and blue) color-model value of the threshold color. This new method simply requires the operator to click on an area of the bitmap for a new threshold, and the RGB value will be extracted from the pixel. If the operator wants to select the threshold value from the background, a dialog will open with the image loaded in the center of the dialog. The operator clicks on the bitmap area with the desired threshold value and closes the dialog. The CBitmapTest application will process the image with the new threshold value.

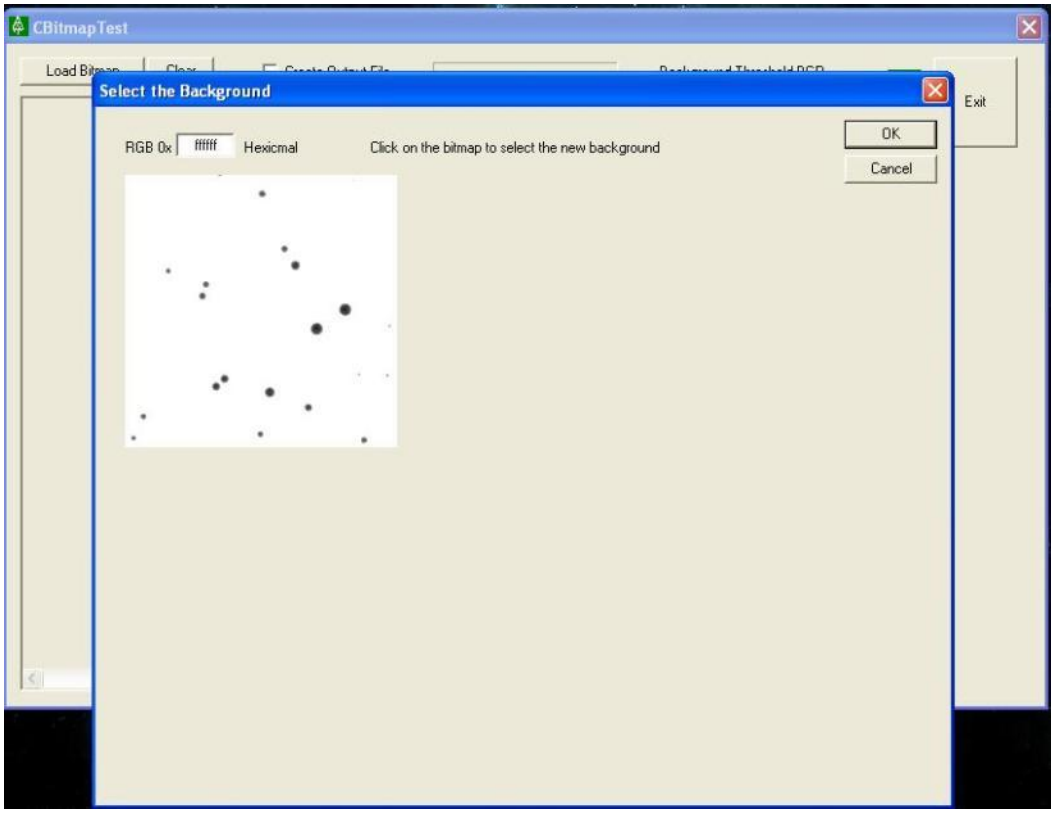

Figure 20. CBitmap background select screen.

6.2 Passive-Imaging Validation Results

Four witness cards were selected to validate the results obtained from software modeling versus the validation effort. The results from each image (Table 6) show close relationship between the modeling and validation.

Table 6. Comparison of Model and Validation for Imaging System

Image Name	Modeling Results (%)	Validation Results (%)	Images
DSC01009	10.6	11.6	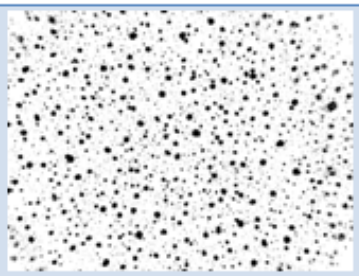
DSC01010	11.3	11.2	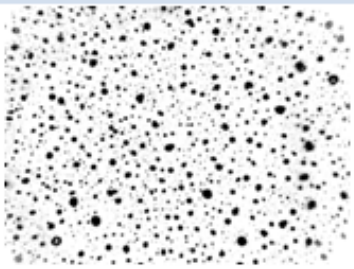
DSC01011	9.4	9.4	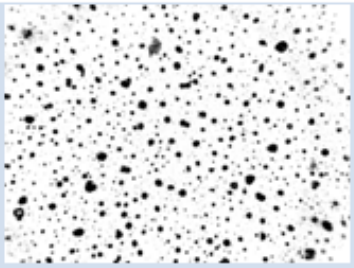
DSC01012	10.2	10.2	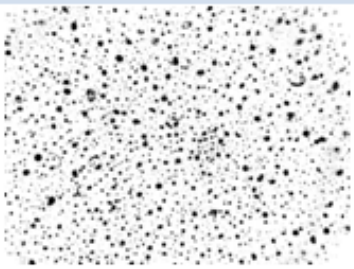

7. 3-D DROPLET MODELING

7.1 Introduction

The wetting action of a liquid drop deposited on a surface depends upon the liquid surface tension, the solid surface tension (surface energy), and the solid–liquid interfacial tension. In this discussion, surface roughness and liquid drop velocity are not considered. It is assumed that the surface is smooth and that the liquid is placed upon the surface. Adhesive forces between the liquid and the solid cause the liquid to spread across the surface. Cohesive forces within the liquid cause the liquid to ball up and avoid contact with the surface. Depending upon the wetting action at the liquid–solid interface, spreading of the puddle may occur with time. This spreading may last for many minutes, which reduces the contact angle. The contact angle is the angle at which the liquid–vapor interface meets the solid–liquid interface. A small contact angle of <90° indicates that surface wetting is favorable, whereas a contact angle of >90° indicates wetting is unfavorable. A surface puddle of low volume assumes the shape of a spherical cap. If the radius of the base of the spherical cap is *a*, and the height of the cap is *h*, then the equation for the volume (*V*) of the spherical cap is

$$V = \frac{\pi h}{6}(3a^2 + h^2) \text{ or } V = \frac{\pi h^2}{3}(3r - h) \tag{4}$$

where *r* is the sphere radius.

As the puddle volume increases, the top of the spherical cap flattens due to the force of gravity. A maximum height is reached as defined in the following equation:

$$h = \sqrt{\frac{2\gamma[1-\cos(\theta)]}{\rho \times g}} \tag{5}$$

where

γ is γ_{LV} the liquid–vapor surface tension,
θ is contact angle,
ρ is liquid density, and
g is gravity acceleration.

Values for liquid–vapor and solid–vapor surface tensions for many materials may be found in the literature. (It should be noted that the published values for solid–vapor surface tension [i.e., surface energy] of many materials such as Teflon coatings and aluminum have been found to be inconsistent, and actual experimental measurements may be more accurate.) Values for solid–liquid surface tensions are usually not readily available but may be derived using the following equation:

$$\gamma_{SL} = \gamma_{SV} + \gamma_{LV} - 2(\gamma_{SV}\,\gamma_{LV})^{1/2} \tag{6}$$

where

γ_{SL} is solid–liquid surface tension, and

γ_{SV} is solid surface tension (solid–vapor).

The contact angle may be derived using the following equation:

$$\gamma_{LV} \times \cos(\theta) = \gamma_{SV} - \gamma_{SL} \quad (7)$$

7.2 Droplet Measurements versus Calculations

The equations presented in this report were applied to drop-shape image analysis data obtained by personnel at the ITT Corporation to verify that these equations were in agreement with actual experimental data. These data were for SF96-5 (poly[oxy(dimethylsilylene)]) on Teflon material. The surface tension for Dow Corning SF96-5 (Dow Chemical Company, Midland, MD) is published as 19.7 dyn/cm; however, the range of published data for Teflon surface energy varies from 18.5 to 20 dyn/cm. The mean ITT experimental contact angle was 23.77°. Solving eq 7 for γ_{SL} and cos(θ), using Teflon surface tensions from 18 to 20 dyn/cm, yields the results shown in Table 7.

Table 7. Calculated Results for SF96-5 on Teflon Material

γ_{SV}	Contact Angle	γ_{SL}
18.00	24.25	.03835
18.06	23.80	.03563
18.10	23.50	.03388
18.25	22.33	.02771
18.50	20.26	.01885
20.00	0	.00113

The calculated contact angles of the droplets, using the assumed range of Teflon surface tensions, include the measured average contact angle of 23.77°, which indicates that the equations are in agreement with the experimental data.

The following calculation was performed to determine whether evaluation of the ITT data indicates the formation of a spherical cap or a cap flattened by gravity. Given the following parameters for a droplet:

- Measured average diameter = 4.826 mm,
- Average height = 0.382 mm,
- Volume = 3.54 mm^2, and
- Radius of spherical cap base = 2.413 mm.

Solving eq 4 (repeated here) for height yields:

$$V = \frac{\pi h}{6}(3a^2 + h^2)$$

$$6.76 = 17.47h + h^3$$
$$h^3 + 0h^2 + 17.613h - 6.589 = 0$$
$$h = 0.384 \text{ mm}$$

The calculated height of a droplet is essentially equivalent to the measured value of 0.382, which indicates that the measured height is consistent with the height of a spherical cap. Equation 5 (repeated here) was used to calculate the maximum height of a droplet where an increased volume would cause a flat top due to gravity:

$$h = \sqrt{\frac{2\gamma[1-\cos(\theta)]}{\rho \times g}}$$

The following parameters were given for a droplet:

- $\gamma_{LV} = 19.7$,
- $\rho = 0.913$ g/mL,
- $g = 980$ cm/s², and
- $\theta = 23.77°$.

Using these values, the maximum height is 0.611 mm.

7.3 Analysis of SF96-5 on Teflon Material

In another aspect of this study, the diameter of a drop of SF96-5 that would produce a 2 in. diameter puddle on a Teflon substrate was calculated. It was assumed that the puddle shape would be a spherical cap with the height and volume to be determined. Theoretical maximum height could be calculated from knowledge of the material characteristics. Whether this maximum height was reached depended upon the liquid volume. A small volume resulted in a spherical cap, whereas a large volume could truncate the cap due to acceleration of gravity.

To calculate the volume of a 2 in. diameter puddle of SF96-5 on Teflon material, the procedure described in this section may be used. Figure 21 represents the cross section of an adjunct sphere, which is used to illustrate a spherical cap that is located at the tangent to a sphere with radius, *r*. The spherical cap has a height, *h*, and a base radius, *a*. Although the sphere does not actually exist, the use of the spherical cap equations in this trigonometric representation allows mathematical solutions for the puddle parameters.

The contact angle, θ, was 22° as described in Section 7.2. Initially, it was assumed that the puddle was a spherical cap. The base of the spherical cap was placed at the point on the sphere corresponding to 22°. Figure 21 shows the sphere's cross section. In this example, the

base of the spherical cap is located at a point on the sphere where a tangent to the sphere is at the contact angle of 22°. Because the base diameter of the spherical cap is 2 in., then the radius is 1 in. or 2.54 cm. The sphere radius forms the hypotenuse of the right triangle. Therefore, the sphere radius is 2.54/cos 68° or 6.781 cm. The height of the spherical cap is $r \times (1 - \sin 68°)$ or 0.4937 cm.

Calculating the maximum height of the spherical cap using eq 6 and θ of 22° yields a height of 0.0566 cm. This indicates that the spherical cap was flattened by gravity, and that the calculated height of 0.4937 cm will not be reached. To calculate the volume of the flattened spherical cap, the volume of the cap with a height of 0.4371 is subtracted from the initial spherical cap with a height of 0.4937.

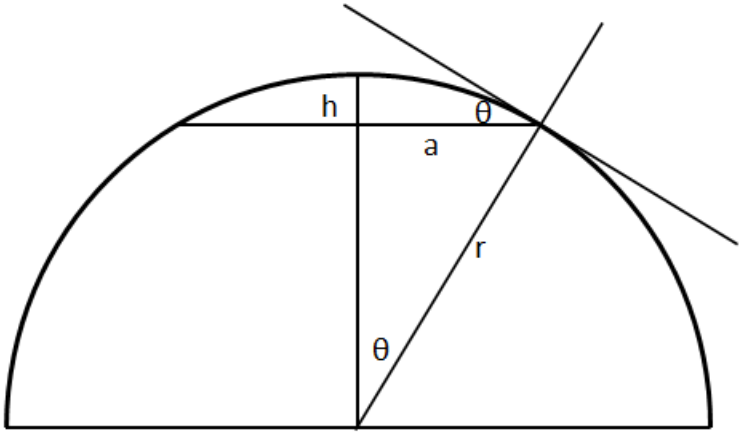

Figure 21. Spherical cap.

Using eq 4 to calculate the volume of a full spherical cap where the height is 0.4937 cm,

$$V = \pi h^2(3r - h)/3 = 5.0664 \text{ cm}^3$$

Similarly to calculate the volume of a spherical cap with a height of .4371 cm,

$$V = \pi h^2(3r - h)/3 = 3.983 \text{ cm}^3$$

Therefore, the volume of the flattened spherical cap

$$V = 5.0664 - 3.983 = 1.083 \text{ cm}^3$$

The diameter, *D*, of a spherical drop of SF96-5 that would produce a 2 in. diameter puddle on Teflon material may then be calculated using the equation for the volume of a sphere

$$V = \pi \times D^3/6 \qquad (8)$$

Using the previously given values in eq 8

$$D^3 = V/0.5236 = 1.0833/0.5236 = 2.068$$

$$D = 1.274 \text{ cm } (0.502 \text{ in.})$$

7.4 Surface Energy of Aluminum

In many references, the published value for sheet aluminum surface energy (surface tension) is 45 dyn/cm; however, this value varies with the aluminum type and surface treatment. Recent studies have indicated an interest in determining the surface energy of the evaporated aluminum film on EMF Corporation (Ithaca, NY) microscope slides. An average value was calculated on the basis of recent experimental data supplied by Dr. Simpson of ITT Corporation (Appendix B). These data were measurements of ethylene glycol droplets on aluminum-coated microscope slides. The data comprised droplet volume, puddle height, diameter, and contact angle. The surface tension of ethylene glycol used in these calculations was the Dow Chemical published value of 48 dyn/cm at 25 °C.

Assuming that the droplets form a spherical cap, eqs 6 and 7 (both repeated here) may be used.

$$\gamma_{SL} = \gamma_{SV} + \gamma_{LV} - 2(\gamma_{SV}\,\gamma_{LV})^{1/2}$$

$$\gamma_{LV} \times \cos(\theta) = \gamma_{SV} - \gamma_{SL}$$

where

γ_{LV} is the liquid–vapor surface tension of ethylene glycol,

γ_{SV} is the solid–vapor surface tension of aluminum, and

γ_{SL} is the solid–liquid surface tension of aluminum–ethylene glycol.

Substituting eq 7 into eq 6 yields

$$\gamma_{SV} = 1/4 \times \gamma_{LV}\,[1+\cos(\theta)]^2 \qquad (9)$$

Using the average measured contact angle as 55.169° and the surface tension of ethylene glycol as 48 dyn/cm, the evaporated aluminum film surface energy is 29.62 dynes/cm.

8. VALIDATION OF DROPLET MODEL

8.1 Predicting the Mass of a Droplet

The droplet-modeling function was used to predict the mass of various solution droplets based on the density, contact angle, surface tension, and gravity acceleration. The first validation experiment was performed using water droplets on a Teflon substrate (Figure 22). Using an imaging microscope, three droplets were measured at 1, 0.5, and 0.25 in. Figure 23 shows the values predicted using modeling and the results recorded during validation.

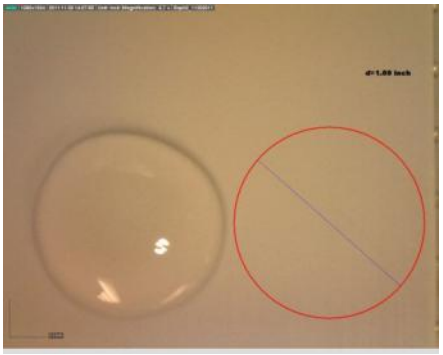

Figure 22. Water droplet on Teflon surface.

	Modeling	Experiment
D = 1 in.	1.89g	1.78g
D = 0.5 in.	0.43g	0.40g
D = 0.25 in	0.069g	0.064g

Figure 23. Comparison of modeling and experimental values for three water droplets on a Teflon surface.

8.2 Predicting the Mass of an EG75 Droplet

The same experiment was continued using EG75, which is a solution of 75% ethylene glycol, 24.5% water, and 0.5% Tween 20 or Polysorbate 20 (Sigma-Aldrich, St. Louis, MO). A droplet representing of 10 µL of EG75 was modeled for the next validation. Modeling predicted a mass of 8.95 mg using the following parameters:

- Contact angle of 30.6° (based on surface tension for brushed aluminum),
- Surface tension of 0.03879 N/m, and
- Density of 1.086 g/mL.

The validation was performed by placing a 10 µL of EG75 solution on an aluminum plate. Pure ethylene glycol was deemed to be too viscous for the Direct Color Systems Direct Jet 1309 printer. However, water was added to ethylene glycol, which brought the viscosity down to 4 cP to yield a solution that could be used in the Direct Jet printers. In this experiment, the droplet was made with a dropper instead of the printer. Using the Dino Capture imaging microscope (Dino-Lite Europe, Naarden, The Netherlands), the EG75 droplet was measured at a diameter of 5.32 mm, and the mass was measured to be 9.0 mg.

8.3 Predicting the Height and Volume of a Droplet

The V&V modeling program can be used to predict the height and volume of a droplet, provided the contact angle and diameter of the droplet are known. To validate this, ITT Corporation personnel conducted a series of droplet tests that measured the volume, diameter, height, and contact angle of a droplet. The ITT data is available in Appendix B. Using the data from the ITT validation test, four droplets were picked at random, and using the equations listed in Section 7, the height and volume were calculated. The model's "makecardprofile.m" module was used to estimate the height and volume of the droplet when provided with the droplet's diameter and contact angle. Three different tests were run: one using a lower resolution, the second using a higher resolution, and the third using an averaged contact angle for all of the droplets tested by ITT personnel. The results are shown in Table 8.

Table 8. Volume and Height Calculations: Modeling vs Measurement

Droplet #		Validation	Model 600 dpi	Model 720 dpi	Model 720dpi
1	Diameter	4.47 mm	105 pixels	126 pixels	126 pixels
	Contact Angle	54.7	54.7	54.7	54.32
	Height (mm)	1.06	1.15	1.15	1.14
	Volume (µL)	8.92	9.68	9.68	9.62
	Error %	-	8.5%	8.5%	7.8%
3	Diameter	4.27 mm	100 pixels	121 pixels	121 pixels
	Contact Angle	54.9	54.9	54.9	54.32
	Height (mm)	1.02	1.10	1.10	1.10
	Volume (µL)	7.81	8.43	8.61	8.52
	Error %	-	8.1%	10.2%	9.0 %
7	Diameter	3.06 mm	72 pixels	86 pixels	86 pixels
	Contact Angle	55.1	55.1	55.1	54.32
	Height (mm)	0.76	0.80	0.79	0.78
	Volume (µL)	2.96	3.14	3.14	3.06
	Error %	-	6.0 %	6.0 %	3.3 %
10	Diameter	1.73 mm	40 pixels	49 pixels	49 pixels
	Contact Angle	54.6	54.6	54.6	54.32
	Height (mm)	0.44	0.44	0.45	0.44
	Volume (µL)	0.52	0.54	0.57	0.56
	Error %	-	9.6 %	9.6 %	7.7 %

9. INKJET PRINTING OF DROPLET DISTRIBUTION

The experimental goal was to print a VLSTRACK-generated droplet distribution onto a solid surface using a chemical simulant. For a 1000 kg of chemical release and 0.5 g/m^2 of coverage, VLSTRACK calculated a total deposit of 20.1 mg of a chemical simulant in a 6 in. square. A plot of the VLSTRACK distribution is provided in Section 9.2.

9.1 Inkjet Printing of SF96-5 on Teflon Material

As an initial printing test, five 10 mm diameter round spots of SF96-5 were printed on a 2 × 2 in. Teflon substrate using the Direct Color Systems Direct Jet 1309 printer. The test pattern is shown in Figure 24, and the results are listed in Tables 9 and 10. This pattern was used to calculate the printer volume per drop.

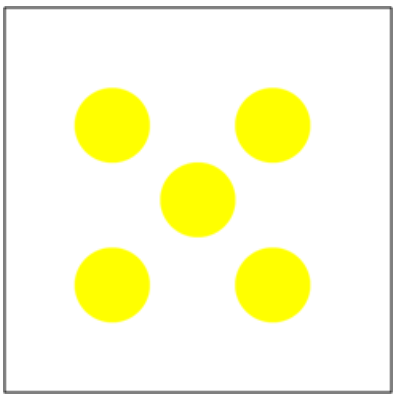

Figure 24. Printing test on a 2 × 2 in. test pattern.

Table 9. SF96-5 in the Yellow Printer Cartridge

Trial	Weight Before Printing (g)	Weight After Printing (g)	Difference (mg)
1	4.79859	4.80206	3.47
2	4.81485	4.81835	3.50

Evaluation of the test results (Table 9) provided the following values:

- Mean weight difference of 3.49 mg,
- Total area of five 10 mm spots equaled 392.7 mm^2,
- at 720 × 720 dpi, the resolution was 518,400 dots/in.^{2} or 803.52 dots/mm^2,
- Total dots were 803.52 × 392.7 = 315,540 dots,
- Weight per dot was $(3.49 \times 10^{-3})/(315.50 \times 10^{3}) = 11.062 \times 10^{-9}$ g,
- SF96-5 density equaled 913 g/L, and
- Volume per droplet was $(11.06 \times 10^{-9})/913 = 12.1$ pL.

This measurement was repeated using SF96-5 in printer cartridge no. 2 (magenta).

Table 10. SF96-5 in the Magenta Printer Cartridge

Trial	Weight Before Printing (g)	Weight After Printing (g)	Difference (mg)
1	4.79959	4.80354	3.95
2	4.81442	4.81828	3.86

Evaluation of the test results (Table 10) provided the following values:

- Mean weight difference of 3.91 mg,
- Total area of five 10 mm spots equaled 392.7 mm^2,

- At 720 × 720 dpi, resolution was 518,400 dots/in.² or 803.52 dots/mm²,
- Total dots equaled 315,540,
- Weight per dot was $(3.91 \times 10^{-3})/(315.50 \times 10^{3}) = 12.393 \times 10^{-9}$ g, and
- Volume per droplet was $(12.393 \times 10^{-9})/913 = 13.57$ pL.

These experimental measurements of droplet volume were significantly less than 21 pL/droplet, which was the amount stated in the printer specifications. However, conditions under which the 21 pL was measured were not disclosed by the printer manufacturer. To potentially increase the droplet volume, an experiment was conducted in which the yellow and the magenta ink cartridges were both used, with each cartridge set to 100% coverage.

Table 11. SF96-5 in the Yellow and Magenta Printer Cartridges

Trial	Weight Before Printing (g)	Weight After Printing (g)	Difference (mg)
1	4.79950	4.80773	8.23
2	4.81850	4.82709	8.59

Evaluation of the test results (Table 11) provided the following values:

- Mean weight difference of 8.41 mg, and
- Volume per droplet was calculated at 29.2 pL.

9.2 VLSTRACK Witness Card

On the basis of the VLSTRACK data, the mass of SF96-5 on a 6 × 6 in. witness card (Figure 25) was 20.1 mg, and the pixel count was 176,980. To calculate the number of coats of SF96-5 that were required to print 20.1 mg of the chemical, we used the following parameters:

- Mass per droplet of $913 \times (29.2 \times 10^{-12}) = 26.7 \times 10^{-9}$ g,
- Mass per coat of $176{,}980 \times (26.7 \times 10^{-9}) = 4.725$ mg per coat, and
- Number of coats equaled 20.1/4.725 = 4.25 coats.

The measured results were:

- Weight of 6 × 6 in. Teflon substrate before printing was 61.0356 g,
- Weight after four coats of SF96-5 was 61.05538 g, and
- Weight difference was 19.78 mg.

This result meets the desired target of 20.1 mg of SF96-5 within 1.6%.

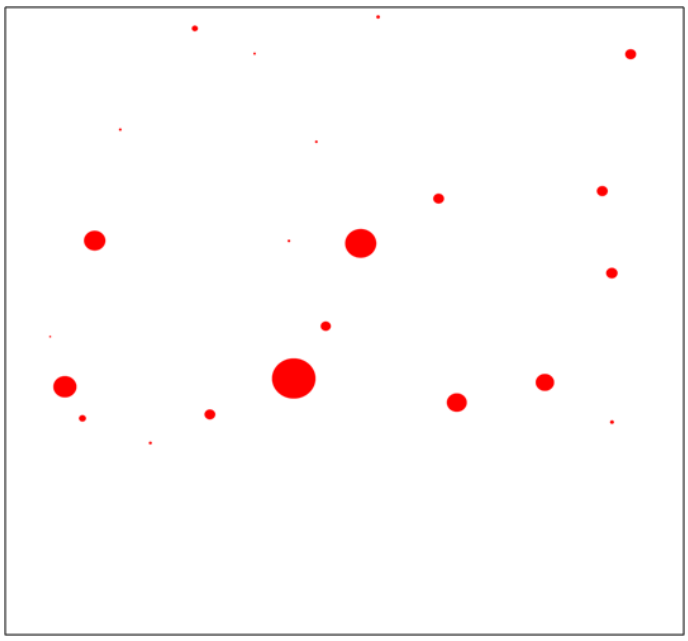

Figure 25. A 6 × 6 in. VLSTRACK card.

10. STANDOFF SURFACE-DETECTION MODEL VALIDATION

A validation system was developed to test the Standoff Surface-Detection model. The system consisted of the Observer Raman system (ObserveR; SciAps, Inc.; Woburn, MA) mounted approximately 1 m above an *x–y* stage. The *x–y* stage was mounted on an optics breadboard. The DeltaNu ObserveR Raman laser was mounted 1 m above the Velmex (Velmex, Inc.; Bloomfield, NY) table. Two computers were used to operate this system (Figure 26). One computer (containing the necessary drivers and software libraries to operate and collect data) controlled the ObserveR, and the other computer controlled the *x–y* stage. Although we were not able to use the ObserveR instrument to print and scan a VLSTRACK droplet pattern due to time constraints, we did demonstrate feasibility by scanning individual droplets of EG75.

10.1 Validation Setup

The ObserveR instrument has an estimated beam diameter of 0.420 mm at 98%, based on a measurement taken by the Coherent Laser Cam II system. The instrument reported a diameter of 0.3 mm at 86.5%.

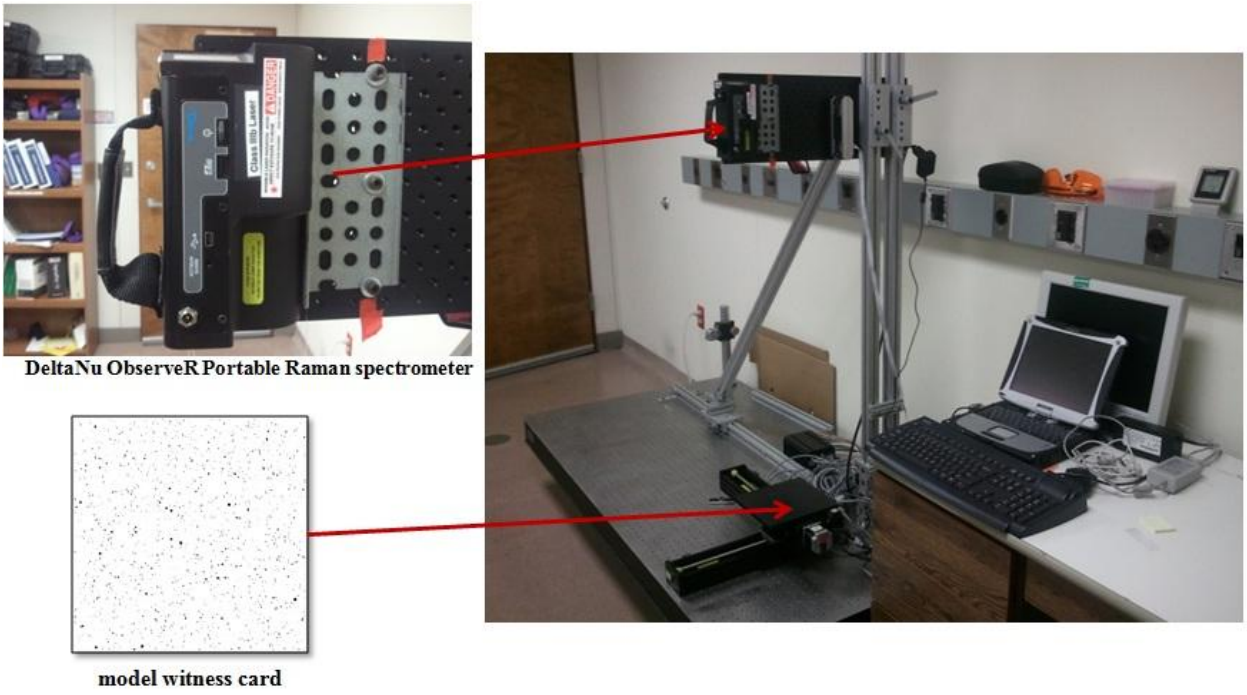

Figure 26. Standoff surface-detection validation setup.

The *x-y* stage consisted of two Velmex BiSlide E04s stacked on top of each other. An 8 × 8 in. table with a tacky pad or C-clamps was used to secure substrates during testing. Software (Figure 27) developed by Hung Technology Solutions, LLC was used to control the *x-y* stage, which allowed the resolution to equal 0.001 in. per step. The Velmex Stepper Motor Controller came with a proprietary programming language. The goal of this application, the surface-detection Velmex table (SDVT), was to hide the proprietary programming language from the operator and provide a simplified graphical user interface (GUI). To move the table, the operator clicked on one of four buttons. The range of each click was variable, with the default movement set to 1 in. At the time of this study, a scan feature was under development that would allow the operator to input a list of points to create a scan pattern. The number of points allowed was set at 100 for this test. Plans to control the laser, named Observer, were also under consideration. The speed setting was based on counts per second, where a value of 1000 equals 1 in./s. The Velmex BiSlide E04 model can travel at speeds up to 6 in./s. The SDVT application sets the speed to 0.5 in./s on initialization. The acceleration is based on a range from 1 to 127, with 127 as the maximum acceleration rate.

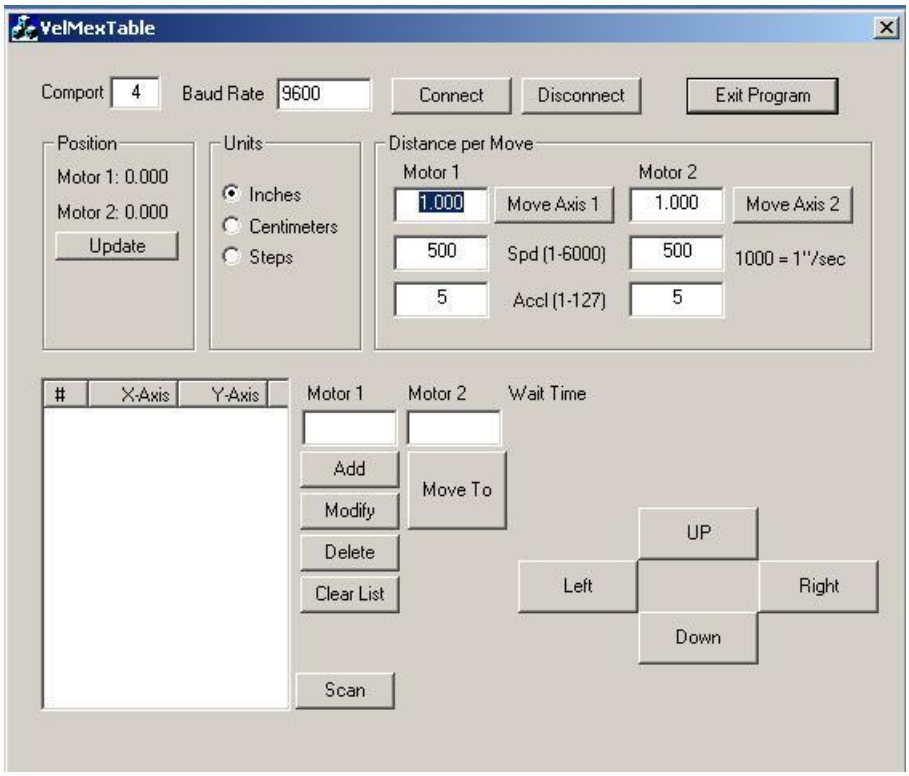

Figure 27. SDVT application.

10.2 Validation of Droplet Model

A droplet consisting of 10 µL of EG75 was deposited on an aluminum plate (Figure 28). The Dino Capture microscope recorded a diameter of 4.748 mm for this drop. Three points were programmed into the SDVT application, and the ObserveR laser was set up to focus on each point (Figure 29).

Figure 28. A 10 µL droplet of EG75 with a diameter of 4.748 mm.

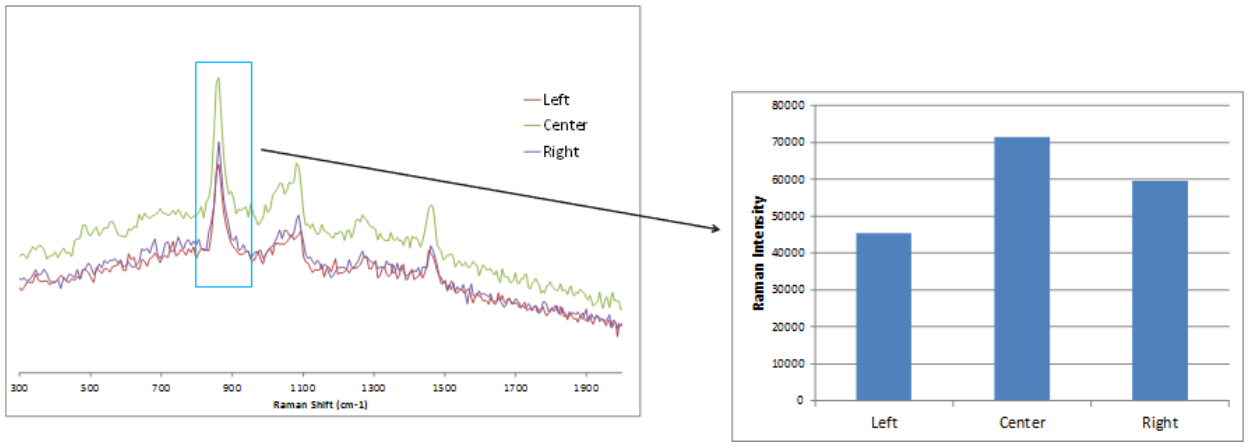

Figure 29. Raman intensity as a function of location on the droplet.

A droplet consisting of 10 µL of EG75 was placed on an aluminum plate. The Dino Capture microscope was used to record a diameter of 4.45 mm for this drop. This time, eight points were used to interrogate this droplet. See Figure 30 for an image of EG75 on aluminum.

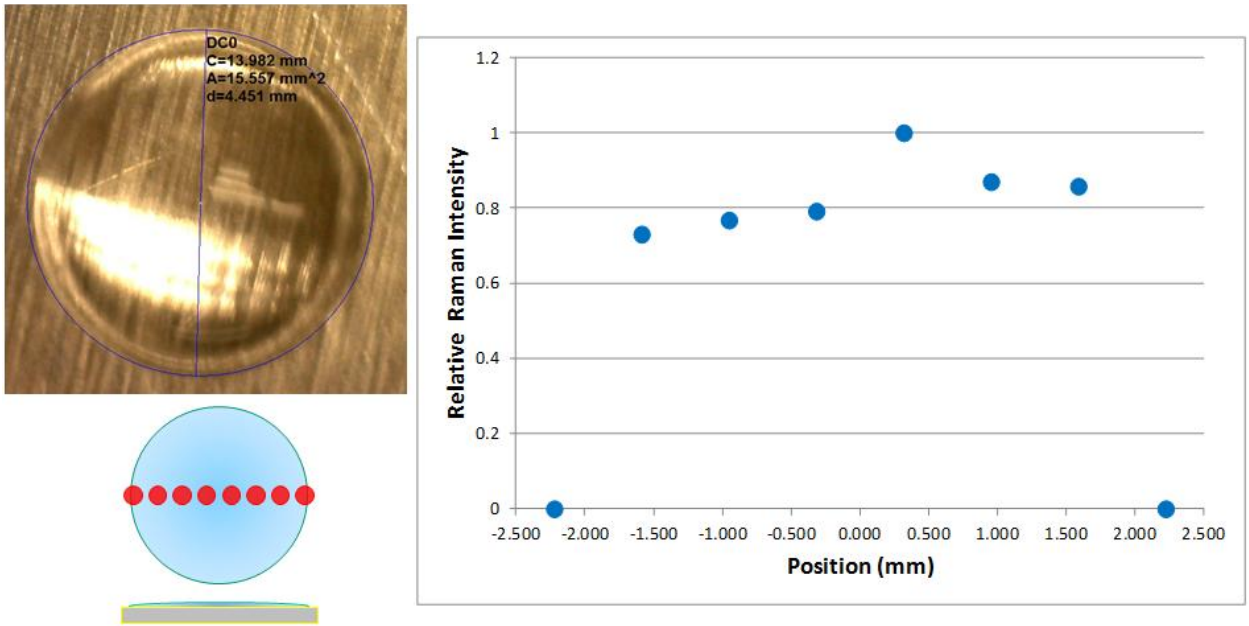

Figure 30. EG75 on aluminum plate.

11. CONCLUSIONS

To support the technology-oriented components of the surface-detection program, ECBC personnel developed a technique to model contaminated droplet distributions on surfaces using realistic values for the chemical fill and delivery system. During this effort, we relied on existing models that accounted for the fate and transport of agent aerosols in the atmosphere and

on experimental data that described the droplet distribution. Use of the chemical and biological agent VLSTRACK computer model provided the team with approximate downwind hazard predictions, droplet distributions, and gross contamination levels for chemical agents and munitions of military interest. We also modeled generic standoff-detection systems using a point-scanning and imaging mode. We validated the models using laboratory measurements and a DoE approach. The goal was a front-to-back modular model that allowed for virtual testing of detection systems and techniques. As part of this program, we also developed an inkjet printing technique for depositing known droplet patterns on surfaces for use in validation studies.

Blank

LITERATURE CITED

1. Bauer, T.; Gibbs, R. *Software User's Manual for the Chemical/Biological Agent Vapor, Liquid, and Solid Tracking (VLSTRACK) Computer Model, Version 3.0*; NSWCDD/TR-98/62; U.S. Naval Surface Warfare Center: Dahlgren, VA, 1998; UNCLASSIFIED Report.

2. Bauer, T.; Young, K.A; Wolski, M. *Final Validation of VLSTRACK Version 3.0, Volume I*; NSWCDD/TR-00/98; U.S. Naval Surface Warfare Center: Dahlgren, VA, 2000; UNCLASSIFIED Report.

3. Moon, R.P.; Guicheteau, J.A.; Christesen, S.D.; Fountain, A.W.; Ginter, J.; Tokarz, J.; Green, N.; Tripathi, A.; Emmons, E.; Hung, K. *Preparation of Chemical Samples on Relevant Surfaces Using Inkjet Technology*; ECBC-TR-1056; U.S. Army Edgewood Chemical Biological Center: Aberdeen Proving Ground, MD, 2013; UNCLASSIFIED Report.

Blank

ACRONYMS AND ABBREVIATIONS

ASCII	American Standard Code for Information Interchange
DoE	design of experiments
ECBC	U.S. Army Edgewood Chemical Biological Center
EG75	75% ethylene glycol, 24.5% water, and 0.5% Tween 20
GUI	graphical user interface
IMG	image (file type)
MMD	mass median diameter
RGB	red, green, and blue
SDK	software development kit
SDVT	surface-detection Velmex table
SF96-5	poly[oxy(dimethylsilylene)
USB	universal serial bus (computer interface)
V&V	verification and validation
VLSTRACK	Vapor, Liquid, and Solid Tracking (computer model)

Blank

APPENDIX A
SCAN MODEL RESULTS FROM CALIBRATION WITNESS CARD

The following data was taken from a single calibration card trial. The trial was a full factorial, where every combination of the relevant parameters was tested. The test parameters included linear scan speed (Scan Speed) at 1.5, 2.5, and 3.5 in./s; laser pulse repetition rate (Repetition Rate) at 10, 100, and 250 Hz; and overlap threshold (Overlap) at 15 and 30%. In addition, there were seven rows of droplets that needed to be scanned one at a time, in which each row had a progressively smaller sized droplet. The droplets were sized at 150, 100, 75, 50, 35, 25, and 15% of the area of the 1.7 mm laser spot. The results of this trial are shown in Figure A-1.

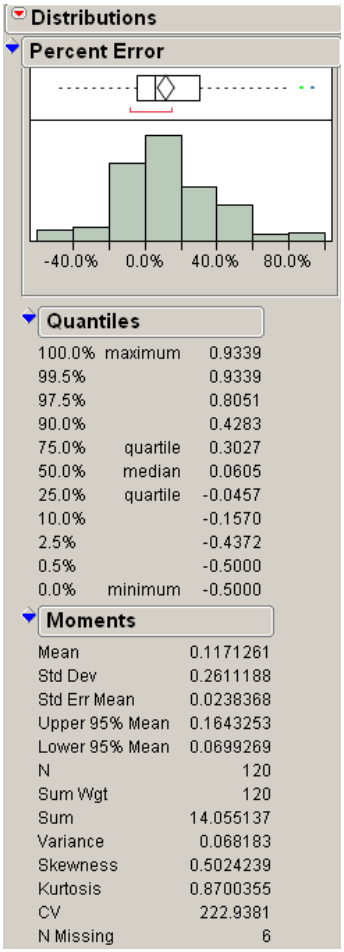

Figure A- 1. Overall error percentage.

Figure A-1 shows a distribution of the error percentage for all 120 test results. This number was obtained by calculating the error between the model results and experimental results. The mean value indicates an overall error percentage of 11.7%, which is good given the small size and large error that were observed in the small droplets making up the final rows.

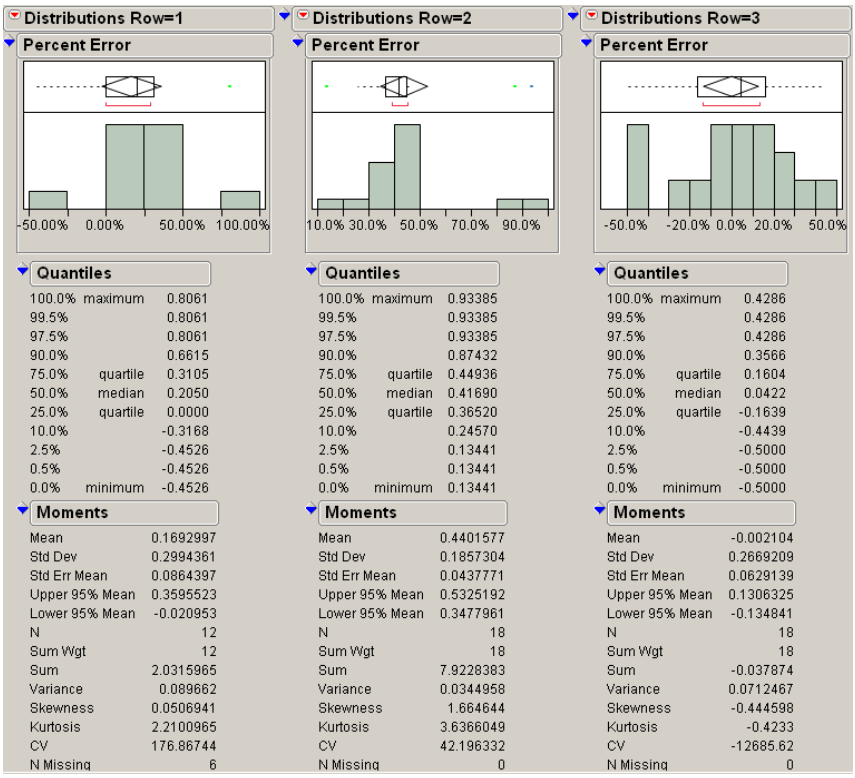

Figure A- 2. Error percentages for rows 1–3.

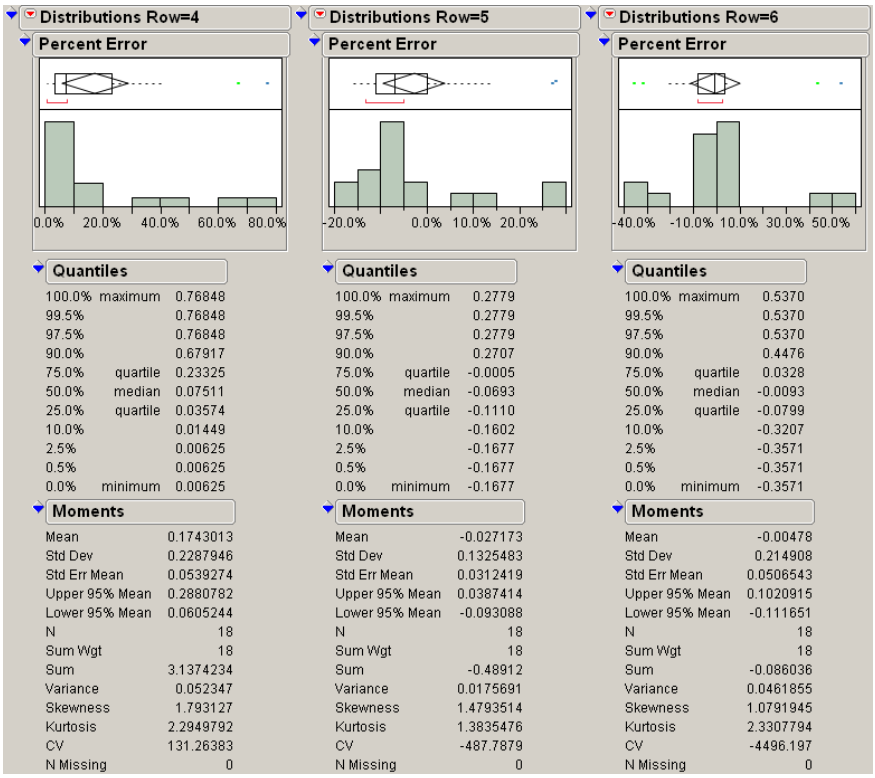

Figure A- 3. Error percentages for rows 4–6.

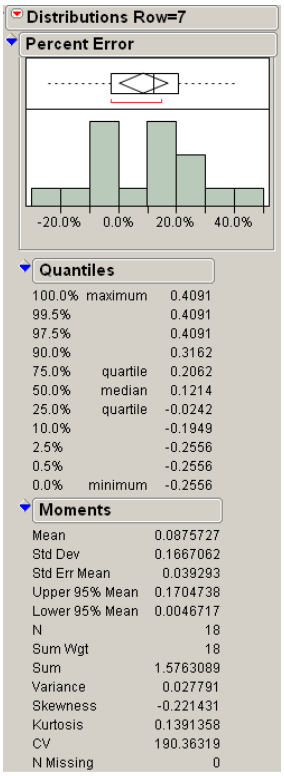

Figure A- 4. Error percentage for row 7.

Figures A-2 through A-4 show the breakdown in error percentage by row. Although there are fluctuations, the trend shows increasing errors with smaller droplet sizes (lower row numbers). Two rows exhibit disagreement of <1%, and only three rows are outside of the 10% goal. Some of the more drastic errors occur in specific rows where the experimental apparatus may not have been fully scanning the rows. This lack of scanning can occur due to the small droplet size and the angular positioning of the gimbal, which causes tracking errors at the ends of certain scan patterns.

Figure A-5 shows the error percentage grouped by overlap threshold. This is effectively a sensitivity setting at this point in time, and results in more hits per shot being recorded. Because the system is more sensitive at lower overlap thresholds, it is easier to record extra hits if the scan pattern strays. This could explain the higher mean error at the 15% overlap setting, but both error rates are close to the target of 10%.

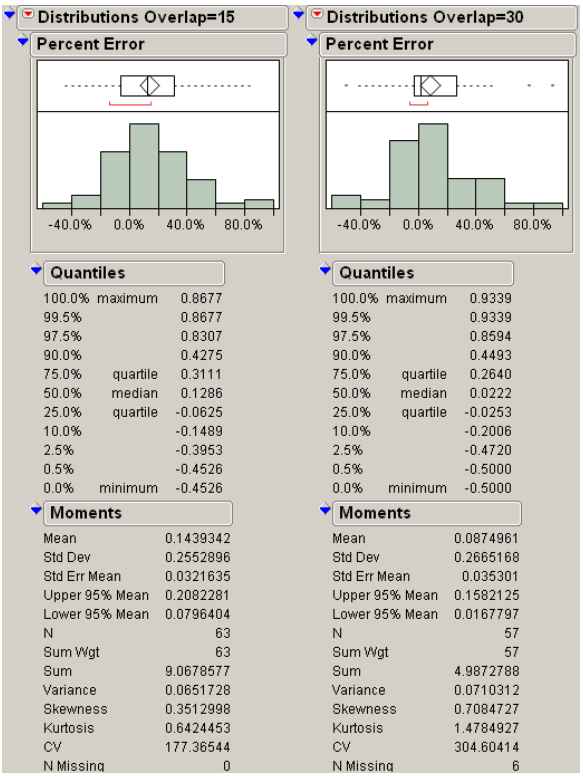

Figure A- 5. Error percentage by overlap setting.

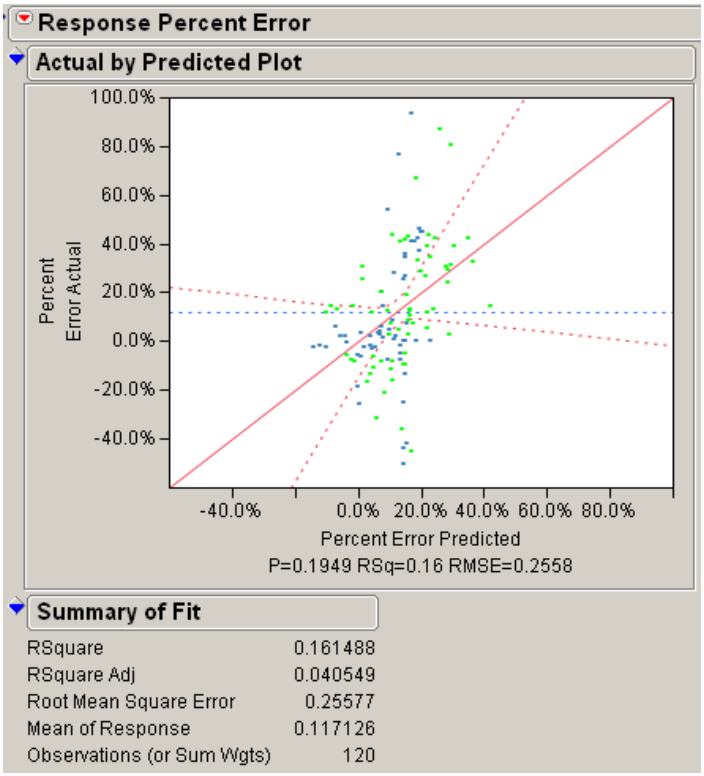

Figure A- 6. Error percentage model.

Figure A-6 shows an actual versus predicted error plot, which graphically illustrates how well a model can predict any errors. The low RSquare value of .16 shows that the model is not a very good fit. This reinforces the positive aspects of our testing because, if a model could reliably predict our error, then the error is not random and distributed across all of our variables. If this were the case, one specific region of data with poor agreement would have to be addressed before proceeding with V&V. Because the RSquare value was low, we can be reasonably certain that there were no major disagreements in the basic functioning of the two systems in this test space.

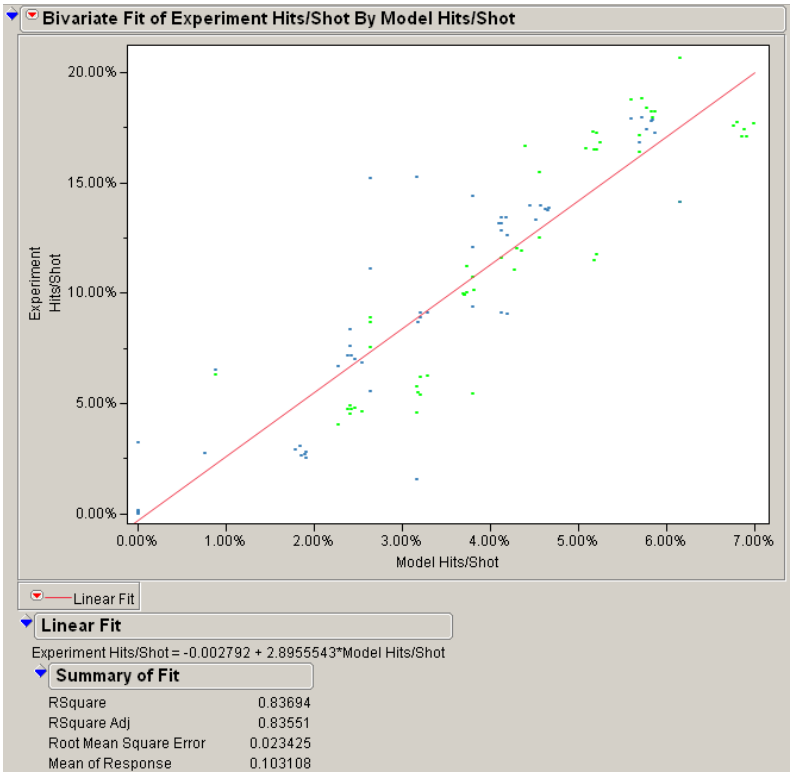

Figure A- 7. Model hits per shot vs experimental hits per shot.

Finally, Figure A-7 shows a comparison of the model hits per shot ratio with the experiment hits per shot. This figure shows a graphical overview comparing the results, but it also displays all of the parameters without normalization, which somewhat skews the general impression regarding the results. The RSquare value of 0.84 shows that there is good agreement between the model and experiment. This situation should improve once a witness card can be scanned freely without concerns about positioning the laser exactly over a specific row of droplets.

Blank

APPENDIX B
CONTACT ANGLE MEASUREMENTS
FOR ETHYLENE GLYCOL ON ALUMINUM

This section provides photographs and plots that were obtained during this study.

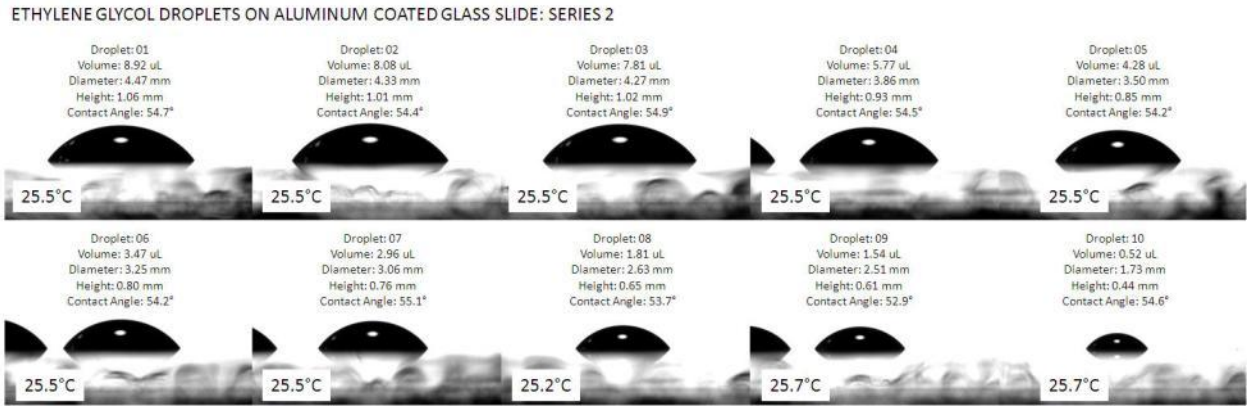

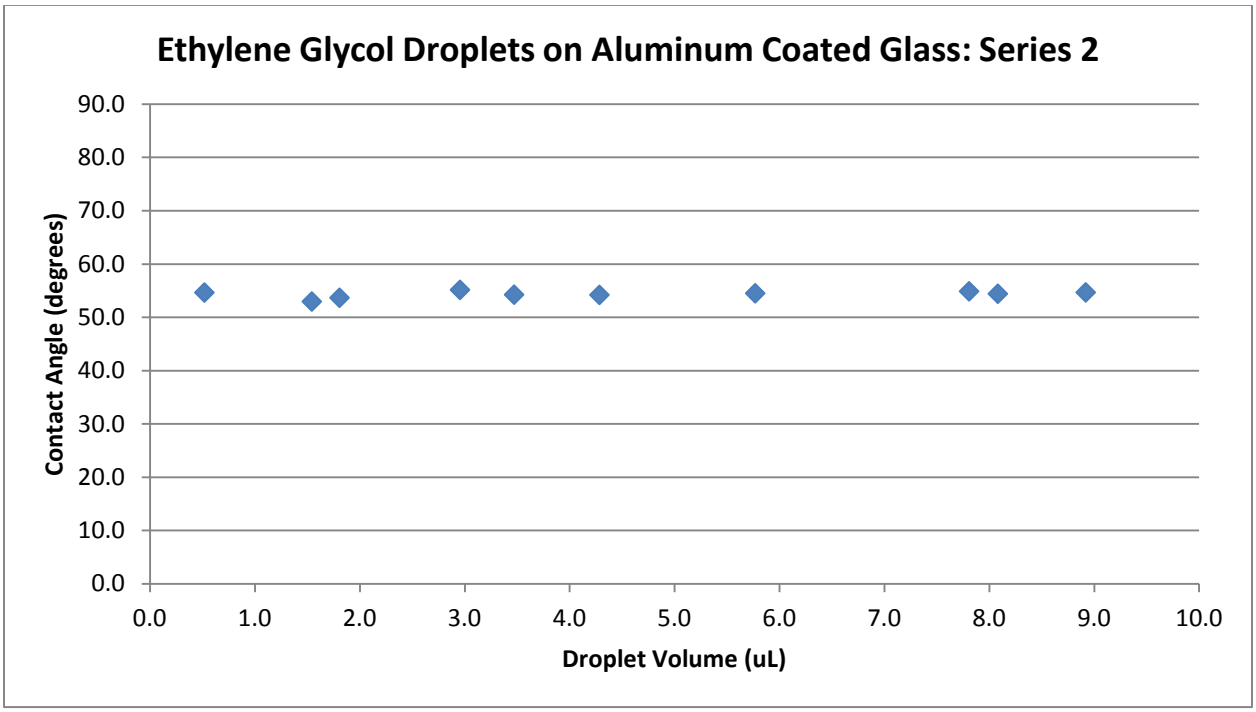

Figure B-1. Ethylene glycol droplets on aluminum-coated glass, Series 2.

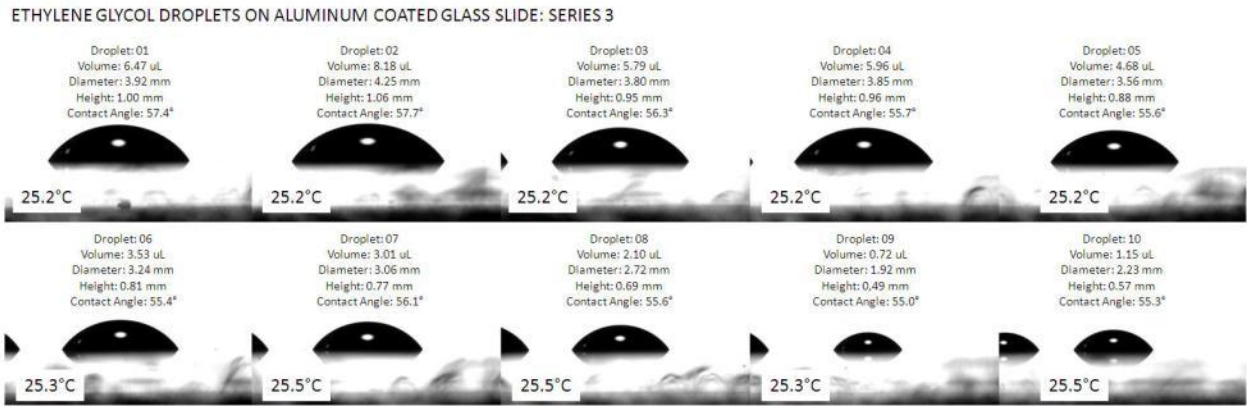

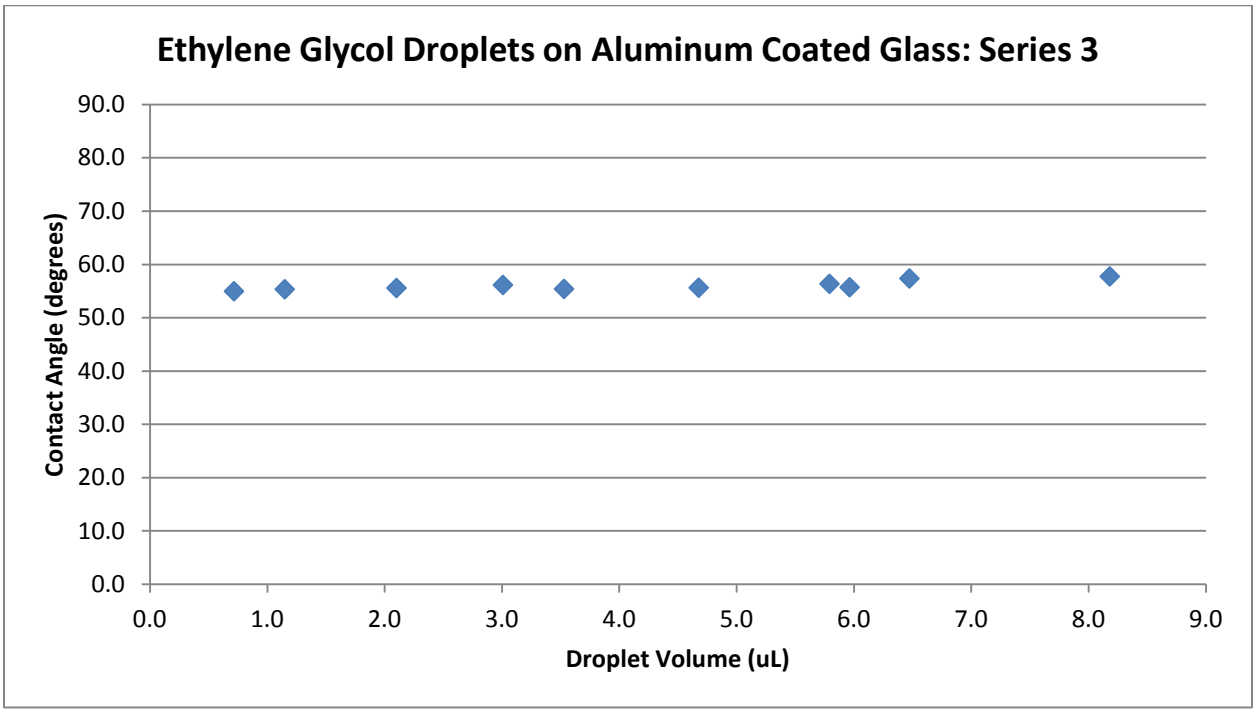

Figure B-2. Ethylene glycol droplets on aluminum-coated glass, Series 3.


EDGEWOOD CHEMICAL BIOLOGICAL CENTER
A U.S. Army RDECOM Laboratory